

**Fractionation of  $^{230}\text{Th}$ ,  $^{231}\text{Pa}$ , and  $^{10}\text{Be}$  induced by particle size and composition within  
an opal-rich sediment of the Atlantic Southern Ocean**

Sven Kretschmer<sup>1, 2\*</sup>, Walter Geibert<sup>3, 4</sup>, Michiel M. Rutgers van der Loeff<sup>1</sup>,  
Christoph Schnabel<sup>5</sup>, Sheng Xu<sup>5</sup>, Gesine Mollenhauer<sup>1, 2</sup>

<sup>1</sup> Alfred-Wegener-Institut für Polar- und Meeresforschung, Am Handelshafen 12, 27570 Bremerhaven,  
Germany

<sup>2</sup> Fachbereich Geowissenschaften, Universität Bremen, Klagenfurter Str., 28359 Bremen, Germany

<sup>3</sup> School of GeoSciences, University of Edinburgh, Edinburgh EH9 3JW, UK

<sup>4</sup> Scottish Association for Marine Science, Dunstaffnage Marine Laboratory, Oban PA37 1QA, UK

<sup>5</sup> Scottish Universities Environmental Research Centre, East Kilbride G75 0QF, UK

\*Corresponding author: sven.kretschmer@awi.de, fax +49 471 4831 1425

## Abstract

This study centers on the question: How sensitive are  $^{231}\text{Pa}/^{230}\text{Th}$  and  $^{10}\text{Be}/^{230}\text{Th}$  to sediment composition and redistribution? The natural radionuclides  $^{231}\text{Pa}$ ,  $^{230}\text{Th}$  and  $^{10}\text{Be}$  recorded in deep sea sediments are tracers for water mass advection and particle fluxes. We investigate the influence of oceanic particle composition on the element adsorption in order to improve our understanding of sedimentary isotope records. We present new data on particle size specific  $^{231}\text{Pa}$  and  $^{10}\text{Be}$  concentrations. An additional separation step, based on settling velocities, led to the isolation of a very opal-rich phase. We find that opal-rich particles contain the highest  $^{231}\text{Pa}$  and  $^{10}\text{Be}$  concentrations, and higher  $^{231}\text{Pa}/^{230}\text{Th}$  and  $^{10}\text{Be}/^{230}\text{Th}$  isotope ratios than opal-poor particles. The fractionation relative to  $^{230}\text{Th}$  induced by the adsorption to opal-rich particles is more pronounced for  $^{231}\text{Pa}$  than for  $^{10}\text{Be}$ . We conclude that bulk  $^{231}\text{Pa}/^{230}\text{Th}$  in Southern Ocean sediments is most suitable as a proxy for past opal fluxes. The comparison between two neighboring cores with rapid and slow accumulation rates reveals that these isotope ratios are not influenced significantly by the intensity of sediment focusing at these two study sites. However, a simulation shows that particle sorting by selective removal of sediment (winnowing) could change the isotope ratios. Consequently,  $^{231}\text{Pa}/^{230}\text{Th}$  should not be used as paleocirculation proxy in cases where a strong loss of opal-rich material due to bottom currents occurred.

# 1. INTRODUCTION

## 1.1 Natural radionuclides and their application as proxies

The natural radionuclides  $^{231}\text{Pa}$ ,  $^{230}\text{Th}$ , and  $^{10}\text{Be}$  are powerful tracers, used to identify and quantify the transport of particles and of water masses in the ocean. The common property of Th, Pa, and Be in seawater is their particle reactivity, which makes them suitable for tracing past particle fluxes. They adsorb onto particles, sink out of the water column (scavenging), and are buried in the sediment. Pa and Be have a lower reactivity and consequently longer residence time than Th. This differing solubility creates disequilibria, and finally leads to isotopic ratios that differ from their production ratio, depending on their residence times in water column.

The production ratios of U-series nuclides are well defined.  $^{230}\text{Th}$  (half-life 75,380 years) is produced by its progenitor  $^{234}\text{U}$  in seawater ( $\sim 2910 \text{ dpm m}^{-3}$  at 35 permil salinity, Robinson et al., 2004) at a constant rate of  $0.0267 \text{ dpm m}^{-3} \text{ a}^{-1}$  (François et al., 2004). Due to its strong particle reactivity (Langmuir and Herman, 1980),  $^{230}\text{Th}$  is adsorbed to colloids or suspended particles shortly after its production in seawater (Moore and Hunter, 1985; Moore and Millward, 1988; Niven and Moore, 1993). The scavenging process for thorium is very efficient so that the rain rate of particulate  $^{230}\text{Th}$  to the sea floor is nearly independent from the intensity of particle fluxes, and thus the vertical  $^{230}\text{Th}$  flux is spatially and temporally constant and equals its production in the overlying water column (within an uncertainty of  $\pm 30\%$ , Henderson et al., 1999; Scholten et al., 2001). Therefore, the residence time of  $^{230}\text{Th}$  in the water column with respect to scavenging is very short (10-40 years, Anderson et al., 1983a, 1983b). Due to its nearly constant vertical flux, the  $^{230}\text{Th}$  concentration in sediments is

25 inversely related to the intensity of the vertical particle flux (Krishnaswami, 1976; Bacon,  
26 1984; Suman and Bacon, 1989).

27         The source of  $^{231}\text{Pa}$  (half-life 32,760 years) in seawater is the radioactive decay of  $^{235}\text{U}$   
28 at a constant rate of  $0.0025 \text{ dpm m}^{-3} \text{ a}^{-1}$ . The activity ratio of  $^{231}\text{Pa}/^{230}\text{Th}$  at the time of  
29 production from  $^{235}\text{U}$  and  $^{234}\text{U}$  is 0.093. However, protactinium is less reactive and has a  
30 longer scavenging residence time than thorium ( $10^2$  years, Anderson et al., 1983a; 1983b).  
31 Therefore,  $^{231}\text{Pa}/^{230}\text{Th}$  ratios may differ from the production ratio in response to the effects  
32 that lead to their removal and transport. In contrast to  $^{230}\text{Th}$ , the distribution of dissolved  $^{231}\text{Pa}$   
33 is largely influenced by lateral mixing and advection of water masses that leads to its further  
34 transport and deposition in regions with enhanced particle fluxes (boundary scavenging,  
35 Anderson et al., 1983a, 1983b). Due to its sensitivity to the hydrography, the  $^{231}\text{Pa}/^{230}\text{Th}$  ratio  
36 in sediments has been interpreted as a record of deep water ventilation in the Atlantic (Yu et  
37 al., 1996; McManus et al., 2004; Gherardi et al., 2009; Guihou et al., 2010; Negre et al., 2010;  
38 Guihou et al., in press).

39         As the  $^{231}\text{Pa}/^{230}\text{Th}$  ratio is positively correlated to the intensity of particle fluxes (Yang  
40 et al., 1986), it has also been applied as an export productivity proxy (Kumar et al., 1993;  
41 Pichat et al., 2004). However, in the Southern Ocean the scavenging of  $^{231}\text{Pa}$  has been found  
42 to be mainly controlled by opal flux (Rutgers van der Loeff and Berger, 1993; Walter et al.,  
43 1997). Therefore, in most recent studies located in high latitudes, the application of  
44  $^{231}\text{Pa}/^{230}\text{Th}$  has been restricted to reconstructing past changes of opal fluxes (Bradtmitter et  
45 al., 2007, 2009; Anderson et al., 2009), rather than total mass fluxes. It is still a matter of  
46 debate if the sensitivity of  $^{231}\text{Pa}/^{230}\text{Th}$  ratios to particle composition affects their application as  
47 paleocirculation tracers, particularly in the North Atlantic. However, modeling results point to  
48 a significant role of particle composition for  $^{231}\text{Pa}/^{230}\text{Th}$  records (Siddall et al. 2005), and the  
49 general lack of larger sets of observational data in combination with useful particle  
50 characterizations is hampering the reliable application of the proxy (Burke et al., 2011).

51  $^{10}\text{Be}$  has a different production mechanism, but certain similarities to  $^{231}\text{Pa}$ . Given its  
52 much longer half-life of 1.5 Million years, it could in principle serve as a welcome extension  
53 of the  $^{231}\text{Pa}/^{230}\text{Th}$  proxy into to the more distant past.  $^{10}\text{Be}$  is produced by spallation reactions  
54 in the troposphere (Lal and Peters, 1967; Lal 2002) at a globally averaged production rate of  
55  $1.2 \times 10^6$  atoms  $\text{cm}^{-2} \text{a}^{-1}$  at present (Monaghan et al., 1986). Once introduced to the ocean,  
56  $^{10}\text{Be}$  does not re-exchange with the atmosphere (Morris et al., 2002) but it is removed from  
57 the water column by scavenging to particles and burial in sediments (Finkel et al., 1977;  
58 Kusakabe et al., 1982; Lao et al., 1992). Owing to its residence time of ~500-1000 years,  
59 dissolved  $^{10}\text{Be}$  is advected laterally in the ocean by water masses and preferentially scavenged  
60 and deposited in regions of high particle flux, similar to  $^{231}\text{Pa}$  (boundary scavenging,  
61 Anderson et al., 1990). Long term records of  $^{10}\text{Be}$  in marine sediments serve as a proxy for  
62 past variations in cosmic ray intensity and for the past geomagnetic dipole strength (Frank et  
63 al., 1997; Frank, 2000; Christl et al., 2007, 2010).  $^{10}\text{Be}$  is also an important tool for sediment  
64 chronology (Bourles et al., 1989; Frank et al., 2008) and for the investigation of water mass  
65 advection (Ku et al., 1990; Frank et al., 2002; Luo and Ku, 2003).  $^{10}\text{Be}$  normalized to the flux  
66 of excess  $^{230}\text{Th}$  ( $^{10}\text{Be}/^{230}\text{Th}_{\text{xs}}$ ) has been used for the reconstruction of variations in the past  
67 ocean productivity (Anderson et al., 1998). The  $^{10}\text{Be}$  flux to marine sediments also varies as a  
68 function of lithology (Henken-Mellies et al., 1990; Chase et al., 2003).

69

## 70 **1.2 The effect of sediment redistribution on nuclide ratios**

71

72 It has been questioned to what extent the sedimentary  $^{231}\text{Pa}/^{230}\text{Th}$  and  $^{10}\text{Be}/^{230}\text{Th}$   
73 records are determined by ventilation versus particle composition. Indeed, recent publications  
74 (Keigwin and Boyle, 2008; Scholten et al., 2008; Gil et al., 2009; Lippold et al., 2009)  
75 claimed that the distribution of  $^{231}\text{Pa}/^{230}\text{Th}$  ratios is controlled at least partly by the abundance  
76 of diatoms and not by ventilation. Various studies have shown that thorium preferentially

77 adsorb on lithogenics and carbonates, beryllium on lithogenics and opal, whereas  
78 protactinium strongly prefers opal (Lao et al., 1993; Chase et al., 2002; Guo et al., 2002;  
79 Chase et al., 2003; Geibert and Usbeck, 2004). The disparity in adsorption behavior and past  
80 changes in particle composition may be disadvantageous for particle flux studies (Frank et al.,  
81 2000; Gil et al., 2009; Lippold et al., 2009), as it is one additional controlling factor on the  
82 tracer flux to the sediment, which may overprint the effect of other controlling factors (such  
83 as total particle flux or water mass advection) and complicate the interpretation of the  
84 sedimentary tracer records (Burke et al., 2011).

85         The opal-rich sediments of the Southern Ocean act as a sink for  $^{231}\text{Pa}$  and  $^{10}\text{Be}$  as a  
86 result from hydrography, scavenging residence times, and chemical composition of oceanic  
87 particles. Opal-rich sediments appear to be particularly susceptible to resuspension, which  
88 makes redistribution by strong abyssal bottom currents particularly important in the opal-belt  
89 of the Antarctic Circumpolar Current (Geibert et al., 2005).  $^{231}\text{Pa}/^{230}\text{Th}$  and  $^{10}\text{Be}/^{230}\text{Th}$  ratios  
90 have been commonly assumed to be insensitive to sediment redistribution, an assumption  
91 which remains to be proven. Focusing and winnowing of sediments occur under the influence  
92 of variable abyssal current velocities. Therefore, laterally transported sediment particles may  
93 be subject to a particle sorting according to particle size and hydrodynamic behavior (McCave  
94 et al., 1995). If distinct particle types with high and low isotope concentrations are decoupled  
95 from one another during a dislocation process, this may potentially change the particulate  
96  $^{231}\text{Pa}/^{230}\text{Th}$  and  $^{10}\text{Be}/^{230}\text{Th}$  ratios in sediments after redeposition, which we can test as part of  
97 this study.

98

### 99 **1.3 Approaches by other authors**

100

101         Generally, data on oceanic  $^{231}\text{Pa}$  and  $^{10}\text{Be}$  are still scarce and beyond that, contrasting  
102 results led to discussions about their interpretation (Luo and Ku, 1999; Chase et al., 2002;

103 Chase and Anderson, 2004; Luo and Ku, 2004a, b). Therefore, a further development of  
104  $^{231}\text{Pa}/^{230}\text{Th}$  and  $^{10}\text{Be}/^{230}\text{Th}$  as quantitative proxies needs more investigation. Various studies  
105 have investigated the scavenging and fractionation of  $^{231}\text{Pa}$ ,  $^{230}\text{Th}$ , and  $^{10}\text{Be}$  with respect to  
106 particle phases. These different approaches include field observations of geographical  
107 variability (e.g. Walter et al., 1997), scavenging experiments under controlled laboratory  
108 conditions (e.g. Geibert and Usbeck, 2004), correlations between radionuclides and sediment  
109 phases in surface sediments (e.g. Lao et al., 1992) or sediment cores (e.g. Henken-Mellies et  
110 al., 1990), studies on the partitioning between dissolved and particulate form in the water  
111 column by collecting suspended or settling particles (e.g. Chase et al., 2002), modeling  
112 studies (e.g. Siddall et al., 2005; Dutay et al., 2009; Luo et al., 2010), and finally component  
113 specific radionuclide analysis by physical or chemical isolation of particle fractions from  
114 sediments (e.g. Bourles et al., 1989; Luo and Ku, 1999; Lal et al., 2006).

115         The methods for component specific radionuclide analysis on isolated sediment  
116 fractions are challenging. The caveat associated with the selective chemical leaching of  
117 sediment phases is the risk of biasing due to desorption/adsorption kinetics of reactive  
118 nuclides from one phase to another (cf. Robinson et al., 2008). Physical separation of  
119 sediment phases by sieving and/or settling bears the problem of incomplete isolation of  
120 sediment phases (cf. Luo and Ku, 1999). The method of wet sieving also could produce an  
121 artifact by an unfavorable leaching of adsorbed isotopes and their loss to the sieving fluid. As  
122 a consequence the component specific radionuclides analyzed on mechanically/chemically  
123 isolated components may not be representative of their natural composition.

124

#### 125 **1.4 How this study addresses the problems**

126

127 This paper contributes new data on component specific radionuclides in order to assess their  
128 sensitivity to redistribution. For our study, we selected two sediment samples (deglacial, 16

129 ka) from two neighboring sediment cores (“twin cores”) from the Southern Atlantic Ocean,  
130 previously described by Kretschmer et al. (2010). While the twin cores are similar in most  
131 respects, they differ in the extent of sediment redistribution. The sample selection is also  
132 advantageous for our study because these samples are mainly composed of only two phases  
133 (opal and lithogenic). Carbonate particles contribute a negligibly small amount (<1 weight-  
134 %). We decided to physically separate those two sediment phases by a gentle treatment (i.e.  
135 without ultrasonication) with natural seawater so that the artificial chemical and physical  
136 influence on radionuclide distribution was reduced to a minimum. Any unfavorable leaching  
137 loss of radioisotopes to the sieve/settle fluid was monitored by analyzing the radioisotopes  
138 within the fluid. Particle separation was achieved by sieving into four size intervals, followed  
139 by a separation through settling velocity into fast and slowly settling particle classes. The fast  
140 settling class mainly contains particles of lithogenic source (higher specific density) and the  
141 slowly settling class mainly contains particles of biogenic opal (lower specific density). Even  
142 though this physical separation was incomplete, the resulting sediment fractions carry  
143 radioisotope signatures that are strongly differing. Kretschmer et. al (2010) had studied  $^{230}\text{Th}$   
144 U and Th in the same size and density fractions of the two cores analyzed in this study, the  
145 new results in this manuscript are on  $^{231}\text{Pa}$  and  $^{10}\text{Be}$ . This paper describes and compares the  
146 distribution of radioisotopes within the sediment samples and the influence of biogenic opal  
147 on the  $^{231}\text{Pa}/^{230}\text{Th}$  and  $^{10}\text{Be}/^{230}\text{Th}$  ratios. The influence of focusing and winnowing on the  
148 isotope ratios and the implication on their use as kinematic proxy for deep water ventilation is  
149 discussed.



## 2. MATERIALS AND METHODS

### 2.1. Sediment core location

Two neighboring sediment cores located in the Southern Ocean opal belt, Atlantic sector south of the Antarctic Polar front (APF), equal in water depth, but different in sedimentation rates were selected for comparison. These two gravity cores (PS1768-8 and PS1769-1) were recovered during Polarstern cruise ANT-VIII/3 at 52.5930°S, 4.4760°E, 3299 m water depth and at 52.6125°S, 4.4580°E, 3269 m water depth, respectively. The sediment composition is dominated by diatomaceous mud and ice rafted debris (Gersonde and Hempel, 1990). Despite the only 2.5 km lateral distance between the twin cores, they reveal contrasting accumulation rates. The sediment deposition during the last deglacial at core site PS1768-8 (mass accumulation rate (MAR)=10.1 g cm<sup>-2</sup> ka<sup>-1</sup>, focusing factor ( $\Psi$ )=5.9; Frank et al., 1996) is twice as high as at core site PS1769-1 (MAR=4.4 g cm<sup>-2</sup> ka<sup>-1</sup>,  $\Psi$ =3.2; Kretschmer et al., 2010), which is assumed to result from lateral sediment transport by bottom currents. The age model of core PS1768-8 is constrained by a combination of oxygen isotope stratigraphy, siliceous microfossil biofluctuation stratigraphy and radiocarbon dating (Frank et al., 1996). Age control for core PS1769-1 was obtained by correlating the magnetic susceptibility record to that of the parallel core. Each of the twin cores was sampled at one core depth (PS1768-8 at core depth 166-169 cm; PS1769-1 at core depth 14-16 cm) representing the last deglacial period (16 ka).

### 2.2. Grain size fractionation

The procedure of the grain size fractionation is reported in detail by Kretschmer et al. (2010). The fractionation of two sediment samples into grain size classes was achieved by wet

176 sieving and settling. Natural seawater (sea surface from the North Sea) was used as sieving  
177 fluid in order to prevent artifacts such as dissolution of particles or desorption of  
178 radionuclides that could result from using deionized water. In order to avoid artifacts from  
179 particles contained in the natural seawater, it was filtered through polycarbonate-filters (pore  
180 size 1  $\mu\text{m}$ ) before using it as a sieving fluid. As this natural seawater contains also  
181 radionuclides of Th, Pa, and Be, which may produce artifacts to the results, the concentration  
182 of radionuclides in the sieving fluid was monitored before and after sediment sieving, as  
183 described in section 2.2.2.

184         The two sediment samples were suspended in filtered seawater and agitated for 2  
185 minutes. The samples were separated into particle size-classes by wet sieving using three  
186 nylon sieves (mesh 125  $\mu\text{m}$ , 63  $\mu\text{m}$ , 20  $\mu\text{m}$ ). Each of the resulting particle size-classes  
187 consisted of particles with different specific densities, i.e. biogenic silica particles (low  
188 density) and lithogenic particles (high density). The size and specific density of a particle  
189 determine its settling velocity and hence its hydrodynamic behavior in a natural marine  
190 system. Therefore, the low density biogenic opal particles were separated from the high  
191 density lithogenic particles by their settling velocity in seawater, so that the three sieve  
192 fractions 20-63  $\mu\text{m}$ , 63-125  $\mu\text{m}$ , and  $>125 \mu\text{m}$  were each split into a “slowly settling” and a  
193 “fast settling” fraction. Two settling velocities were specified: the maximum terminal velocity  
194 (fast sinking particles) was estimated assuming the average density of quartz ( $2.65\text{g cm}^{-3}$ ), the  
195 minimum terminal velocity (slowly sinking particles) was determined empirically by  
196 measuring settling times of the slowest particles in a settling tube with seawater. Shortly after  
197 the fast particles settled down to the bottom of the settling tube the slowly particles were  
198 siphoned off. The fraction that rapidly settled to the bottom was again suspended and the  
199 separation process was repeated (15-20 times) until the supernatant fluid appeared clear.

200         The separation of the  $<20 \mu\text{m}$ -fraction into clay-sized particles ( $<2 \mu\text{m}$ ) and silt-sized  
201 particles (2-20  $\mu\text{m}$ ) was impossible when using seawater, as the smallest particles were

202 flocculating due to the presence of cations in seawater. For further fractionation into the  
203 classes  $<2\ \mu\text{m}$  and  $2\text{-}20\ \mu\text{m}$  based on the settling velocity principle the  $<20\ \mu\text{m}$ -fraction was  
204 resuspended in purified water. After a certain settling time (calculated by Stokes' law), the  
205 clay-sized fraction ( $<2\ \mu\text{m}$ ) remaining in suspension was siphoned off, while the fine silt  
206 fraction ( $2\text{-}20\ \mu\text{m}$ ) settled out from suspension to the bottom of the settling tube and was  
207 again resuspended in purified water. This procedure was repeated 10-20 times until the  
208 supernatant fluid achieved a low turbidity. Due to the repeated decantations the clay-sized  
209 fraction ( $<2\ \mu\text{m}$ ) was recovered in a large volume of water. As flocculation reagent, a  $\text{CaCl}_2$ -  
210 solution was added for extracting all particles from the water. The flocculated particles were  
211 allowed to settle down for four days, and then supernatant was decanted and stored separately  
212 in a canister for further processing (section 2.2.2).

213

#### 214 *2.2.1 Characterization of the grain size fractions*

215

216 Further analyses of the sediment fractions include the measurement of biogenic opal  
217 (bSi), specific surface area (SSA), and element concentrations. Results were reported by  
218 Kretschmer et al. (2010) and are listed in the appendix in Tables A2 and A3.

219 The determination of biogenic opal (bSi) followed the description of Müller and  
220 Schneider (1993) where opal was extracted with NaOH (1 M) at  $85^\circ\text{C}$ , and dissolved silica  
221 was continuously analyzed by molybdate-blue spectrophotometry. The main characteristic of  
222 the slowly settling particles is its high concentration of biogenic opal (mainly diatom tests,  
223 75-82 wt-%). Also the fine silt ( $2\text{-}20\ \mu\text{m}$ ) and the clay-sized ( $<2\ \mu\text{m}$ ) particle fractions  
224 contain high amounts of opal (mainly fragments of diatom tests, 76-80 wt-% respectively 61-  
225 68 wt-%). In contrast, the fast settling particles with lower opal content (3-17 wt-%) contain  
226 mainly ice rafted rock fragments, mixed with radiolarians and few diatoms.

227 Element concentrations (Be, Al, Fe, Mn) have been analyzed on the samples after full  
228 acid digestion using the ICP-SF-MS Element2 (Thermo Scientific). Calibrations were done  
229 with certified standard solutions and external reproducibility was monitored using the NIST  
230 standard reference material 2702 (inorganics in marine sediment). Fe-Mn oxyhydroxides in  
231 the form of coatings or micronodules are known to scavenge both Pa and Th (Anderson et al.,  
232 1983a and references therein; Anderson et al., 1994; Roy-Barman et al., 2005, 2009) and  
233 could therefore play an important role for the grain size distribution of isotopes in sediments.  
234 However, we have no evidence for the existence of Fe-Mn oxyhydroxides in the samples  
235 analyzed. It seems that Fe-Mn oxyhydroxides are of minor importance for our study as  
236 concentrations of Fe and Mn show no correlation to concentrations of Th, Be or Pa. Data on  
237 Fe and Mn were reported by Kretschmer et al. (2010).

238 The specific surface area [ $\text{m}^2 \text{g}^{-1}$ ] of sediment fractions from PS1769-1 was  
239 determined by gas adsorption analysis on a Quantachrome *Nova 2200*. The sediment samples  
240 were degassed and heated ( $110^\circ\text{C}$  for 2h) to remove surface adsorbed water. After evacuation,  
241 the sediment was subjected to five partial pressures of  $\text{N}_2$  gas (purity 99.996%) and the  
242 surface area was calculated using the BET-theory (Brunauer et al., 1938) according to  
243 ISO9277.

244

### 245 2.2.2 Seawater processing

246

247 The use of natural seawater as sieving fluid could provoke artifacts on the radionuclide  
248 concentrations on the sieved sediment particles resulting from adsorption- or desorption-  
249 effects. Therefore radionuclide concentrations were determined in the sieving fluid before it  
250 was used for the wet sieving process (i.e. “unused” seawater) and after the wet sieving of the  
251 sediment samples. The seawater used for wet sieving was collected in canisters (between 11 L  
252 and 22 L per sieved sample, Table 1). Prior to analysis, all seawater samples were acidified

253 (pH 2-3) by addition of nitric acid (HNO<sub>3</sub>). The yield tracers <sup>229</sup>Th, <sup>233</sup>Pa, <sup>236</sup>U, <sup>9</sup>Be, and a  
254 solution of iron chloride were added. After time for equilibration (24 h) ammonium hydroxide  
255 (NH<sub>4</sub>-OH) was added to adjust a pH 8-9 for co-precipitating the radionuclides with iron  
256 hydroxide (Fe(OH)<sub>3</sub>). The precipitate was re-dissolved in HNO<sub>3</sub> and ion exchange chemistry  
257 was performed following the same protocol as for the sediment samples (section 2.3).

258 The results in Table 1 show that after sediment sieving the radionuclide concentrations  
259 in the sieving fluid were higher than before sieving. The difference is assumed to be the  
260 amount that was leached from sediment during the sieve/settle process. It accounts for 0.4-2.4  
261 % relative to the total amount of <sup>230</sup>Th, <sup>231</sup>Pa and <sup>10</sup>Be within the respective bulk sample.

262

### 263 2.2.3 *Recovery of <sup>230</sup>Th, <sup>231</sup>Pa, and <sup>10</sup>Be during sediment sieving*

264

265 The isotope recoveries after sediment sieving are calculated by summing up the <sup>230</sup>Th,  
266 <sup>231</sup>Pa, and <sup>10</sup>Be concentrations of all particle size fractions and dividing by the concentration  
267 of the respective bulk sample. Recoveries of <sup>230</sup>Th, <sup>231</sup>Pa, and <sup>10</sup>Be in sediment fractions sum  
268 up to, respectively, 87-90 %, 109-110 %, and 103-104 % relative to the bulk sample (Table  
269 1).

270

271

## 272 **2.3. Radioisotope analyses**

273

274 The analyses of <sup>231</sup>Pa, <sup>230</sup>Th, and <sup>10</sup>Be were performed in the laboratories of the Marine  
275 Geochemistry department at Alfred-Wegener-Institute, Bremerhaven, Germany and the  
276 NERC Cosmogenic Isotope Analysis Facility (CIAF) and AMS laboratory, both at the  
277 Scottish Universities Environmental Research Center (SUERC), East Kilbride, UK. These  
278 laboratories participated in the GEOTRACES inter-calibration program for <sup>231</sup>Pa, <sup>230</sup>Th and

279  $^{10}\text{Be}$  (Henderson et al., 2007). The data on  $^{231}\text{Pa}$  ( $T_{1/2}=32.5$  ka),  $^{230}\text{Th}$  ( $T_{1/2}=75.4$  ka), and  $^{10}\text{Be}$   
280 ( $T_{1/2}=1.5$  Ma) reported in this manuscript are decay-corrected for the time of deposition. All  
281 data are available at [doi:10.1594/PANGAEA.759976](https://doi.org/10.1594/PANGAEA.759976).

282

### 283 2.3.1. $^{231}\text{Pa}$ sample preparation and ICP-MS

284

285 For the isotope dilution analysis by Inductively Coupled Plasma-Sector Field-Mass  
286 Spectrometry (ICP-SF-MS) the samples were spiked with  $^{229}\text{Th}$ ,  $^{233}\text{Pa}$  and  $^{236}\text{U}$ . The  
287 protactinium spike  $^{233}\text{Pa}$  was produced from a  $^{237}\text{Np}$  solution by separating  $^{233}\text{Pa}$  from its  
288 progenitor by chromatography on a silica gel column. The spikes  $^{229}\text{Th}$ ,  $^{233}\text{Pa}$  and  $^{236}\text{U}$  were  
289 calibrated against the reference standard material UREM 11, an uranium ore. Hansen and  
290 Ring (1983) established that this material is in state of radioactive equilibrium. The consensus  
291 value for the uranium concentration in UREM 11 is  $58.9\pm 0.5$  ppm (Hansen and Ring, 1983).  
292 From this value, we deduced the concentrations of  $^{238}\text{U}$  ( $58.48\pm 0.50$  ppm),  $^{234}\text{U}$  ( $3.16\pm 0.03$  ng  
293  $\text{g}^{-1}$ ) and  $^{235}\text{U}$  ( $418.8\pm 3.6$  ng  $\text{g}^{-1}$ ) and calculated the concentrations of the respective daughter  
294 nuclides  $^{230}\text{Th}$  ( $957.3\pm 8.2$  pg  $\text{g}^{-1}$ ) and  $^{231}\text{Pa}$  ( $19.16\pm 0.16$  pg  $\text{g}^{-1}$ ).

295 Samples (10-100 mg) and spikes (0.7 pg  $^{233}\text{Pa}$ , 9 pg  $^{229}\text{Th}$ , and 800 pg  $^{236}\text{U}$ ) were  
296 weighed into Teflon vials and fully dissolved in HCl, HNO<sub>3</sub>, and HF by microwave-assisted  
297 digestion (CEM Mars Xpress). Samples were evaporated to dryness, re-dissolved, and co-  
298 precipitated with Fe(OH)<sub>3</sub>. Separation of Pa, Th and U was achieved by ion exchange  
299 chromatography with two different exchange resins (Eichrom UTEVA® and BioRad AG 1-  
300 X8®). The UTEVA columns were conditioned with three column volumes (cv) HNO<sub>3</sub> (3M),  
301 then loaded with the samples and rinsed with HNO<sub>3</sub> (3cv 3M). Th was eluted with HCl (1cv  
302 9M and 2cv 5M suprapur®) followed by elution of Pa and U with 3cv HCl (0.02M) + HF  
303 (0.02M suprapur®). The eluates were collected and evaporated in Teflon beakers. The Th  
304 fraction was re-dissolved in HNO<sub>3</sub> and as the last step diluted to 5 mL HNO<sub>3</sub> (1M). The Pa-U

305 fraction was re-dissolved in HCl (9M). The AG 1-X8 columns were conditioned with HCl  
306 (9M) and loaded with the Pa-U fraction. The first rinsing (3cv HCl 9M) cleaned the column  
307 from any remaining Th and was discarded. Subsequently it was collected for Pa (3cv HCl 9M  
308 + HF 0.14M) and for U (5cv HCl 0.5M). The separated Pa and U fractions were evaporated  
309 and re-dissolved in HNO<sub>3</sub> twice, and finally diluted to 5 mL HNO<sub>3</sub> (1M).

310           Isotopes of Pa, Th and U were analyzed by isotope dilution using ICP-SF-MS  
311 (Element2, Thermo Scientific). Samples were injected into the plasma by a desolvation  
312 system (Apex Q<sup>®</sup>, ESI). During the injection of the Pa fraction, Th hydride (<sup>232</sup>ThH<sup>+</sup>)  
313 formation may contribute to the mass 233. This was reduced to a minimum by optimizing the  
314 sample and Argon gas flow rates and the plasma temperature. In addition, the <sup>232</sup>Th peak  
315 tailing contributes to the masses 233 and 231. The external measurement of a <sup>232</sup>Th standard  
316 solution allowed the assessment of these analytical effects. The contribution to masses 231  
317 and 233 by <sup>232</sup>ThH<sup>+</sup> and <sup>232</sup>Th peak tailing was corrected by measuring the <sup>232</sup>Th in each Pa  
318 sample. The instrument mass bias was assessed externally by bracketing samples with a  
319 uranium standard solution. Further corrections accounted for <sup>233</sup>U bleeding (traced by <sup>236</sup>U)  
320 and procedural blanks. Procedural blanks (including spike contribution) were equivalent to  
321 0.8-3% (<sup>231</sup>Pa) and 0.6% (<sup>230</sup>Th) of the samples.

322           The scavenging process is the principal source for <sup>230</sup>Th and <sup>231</sup>Pa in sediments.  
323 Additionally, two further sources contribute variable small amounts to the total <sup>230</sup>Th and  
324 <sup>231</sup>Pa in sediments: <sup>230</sup>Th and <sup>231</sup>Pa that is supported by decaying uranium in lithogenic  
325 minerals, and by decaying uranium from authigenic source. For particle flux studies, only the  
326 scavenged component of <sup>230</sup>Th and <sup>231</sup>Pa is of interest, i.e. the total <sup>230</sup>Th and <sup>231</sup>Pa measured  
327 in sediments must be corrected for the other two components. The scavenged fraction is  
328 referred to as “excess” (excess <sup>230</sup>Th or <sup>230</sup>Th<sub>xs</sub> and excess <sup>231</sup>Pa or <sup>231</sup>Pa<sub>xs</sub>) and must be decay  
329 corrected for the time of deposition which requires an independent chronology for the  
330 sediment core (Henderson and Anderson, 2003).

331

332 2.3.2. <sup>10</sup>Be sample preparation and AMS

333

334 <sup>10</sup>Be was analyzed on 12 sediment samples (2×bulk + 10×fractions) and four  
335 seawater samples. The size classes <2 μm and 2-20 μm were not analyzed separately but were  
336 combined for a measurement of the fraction <20 μm. The size classes 63-125 μm and >125  
337 μm were combined for a measurement of >63 μm. About 390 μg Be (in 3 wt-% HNO<sub>3</sub>) was  
338 added to the sediment samples (~100 mg) prior to the microwave-assisted full acid digestion.  
339 After sample digestion, the acid was fumed off until dryness and samples were re-dissolved in  
340 HCl (3 mL, 6 M) twice. The four acidified (pH 2-3) seawater samples (2×supernatant sieving  
341 fluid and 2×"unused" seawater, for details see section 2.2.2) were prepared for <sup>10</sup>Be  
342 measurement by adding 2 mL solution of iron chloride (FeCl<sub>3</sub> in HCl, 50mg/mL) and 390 μg  
343 Be (in 3 wt-% HNO<sub>3</sub>). After 24 h of equilibration aqueous ammonia was added until pH 10  
344 was reached and Be was co-precipitated with Fe(OH)<sub>3</sub> and Mg(OH)<sub>2</sub>. The supernatant was  
345 siphoned off and the precipitate was re-dissolved in HCl. After three times of co-  
346 precipitations the sample volume was ~30 mL. It was further reduced to ~3 mL by  
347 evaporation on hotplates.

348 Samples (in HCl, 3 mL, 6 M) were loaded on basic anion exchange resin (Merck,  
349 Dowex 1-X8, 2 mL), eluted with HCl (3 cv, 6 M), and immediately collected for Be. Fe is  
350 bound to the resin as FeCl<sub>4</sub><sup>-</sup>-anion. As the Fe content in the seawater samples was very high  
351 due to the Fe(OH)<sub>3</sub>-co-precipitation, each seawater sample was split into two fractions and  
352 anion exchange was repeated using a large column (5 mL resin) for each sample split. After  
353 anion exchange the sample splits were combined again before the next step.

354 Samples were converted into sulfate form by adding H<sub>2</sub>SO<sub>4</sub> (1 mL 0.5 M,  
355 analytical grade) and evaporating to near dryness. H<sub>2</sub>O<sub>2</sub> (6 drops 2 wt %) and H<sub>2</sub>SO<sub>4</sub> (2 mL  
356 0.04 M) were added and evaporated two times to a syrupy droplet. The sample was re-



357 dissolved in H<sub>2</sub>SO<sub>4</sub> (2 mL 0.04 M), let stand overnight and centrifuged before loading to the  
358 cation exchange columns. The “fast settling” particle fractions were estimated to contain high  
359 cation loads (particularly Na<sup>+</sup>, Mg<sup>2+</sup>, Ca<sup>2+</sup>, Al<sup>3+</sup>, and TiO<sup>2+</sup>), so that they were split onto two  
360 columns (each 2 mL) in parallel. All other samples were separated on one column. Samples  
361 were loaded on a sulfonic acid cation exchange resin (BioRad, AG 50W-X8 Resin, 2 mL,  
362 200-400 mesh) conditioned with 0.2 M H<sub>2</sub>SO<sub>4</sub>. Then the TiO<sup>2+</sup>-containing fraction was eluted  
363 from the resin with H<sub>2</sub>SO<sub>4</sub> (6 cv 0.5 M), followed by elution of Be<sup>2+</sup> with HCl (5 cv 1.2 M),  
364 and Al<sup>3+</sup> was removed from the resin with HCl (3 cv 4.5 M).

365           The Be-fraction was reduced to a small volume (~1 mL) by evaporation and  
366 Be(OH)<sub>2</sub> was precipitated at pH 9 by adding an aqueous NH<sub>3</sub> solution (25 wt-%). The  
367 precipitate was centrifuged and washed with pH 7 solution (1 mL) three times, dissolved in  
368 concentrated HNO<sub>3</sub> (60 μL 70 %, certified) and transferred to quartz crucibles. Samples were  
369 dried down on a hotplate, and Be(NO<sub>3</sub>)<sub>2</sub> was partly decomposed by increasing the temperature  
370 to above 200°C. For conversion to BeO the samples were heated in a furnace to 900°C.

371           For the AMS analysis BeO was mixed with Niobium (~4 mg, purity 99.99%, Alfa  
372 Aesar, 325 mesh; mixing ratio BeO/Nb = 1:6 wt/wt) and pressed into a Cu cathode. The  
373 <sup>10</sup>Be/<sup>9</sup>Be ratios that resulted after carrier addition were measured with the 5 MV accelerator  
374 mass spectrometer at SUERC (Freeman et al., 2007). The measurement is described in detail  
375 by Xu et al. (2010). NIST SRM4325 with a <sup>10</sup>Be/<sup>9</sup>Be ratio of 3.06×10<sup>-11</sup> (Middleton et al.,  
376 1993) was used for normalization.

### 3. RESULTS AND DISCUSSIONS

#### 3.1. Protactinium

The fast sinking coarse particles  $>20\ \mu\text{m}$  (opal-poor) are characterized by very low  $^{231}\text{Pa}_{\text{xs}}$  specific activities ( $0.03\pm 0.01 - 0.19\pm 0.03$  dpm/g, Figure 1, Table A1 in the Appendix), and by  $^{231}\text{Pa}_{\text{xs}}/^{230}\text{Th}_{\text{xs}}$  activity ratios ( $0.013\pm 0.003 - 0.05\pm 0.01$ ) lower than the production ratio (0.093). In contrast, the slowly sinking coarse particles  $>20\ \mu\text{m}$  (opal-rich) and the fine particles  $<20\ \mu\text{m}$  (opal-rich) reveal high specific activities ( $0.46\pm 0.08 - 1.89\pm 0.32$  dpm/g) and their  $^{231}\text{Pa}_{\text{xs}}/^{230}\text{Th}_{\text{xs}}$  activity ratios ( $0.11\pm 0.03 - 0.54\pm 0.13$ ) are similar to or higher than the production ratio.

Bulk  $^{231}\text{Pa}_{\text{xs}}$  activities ( $1.10 \pm 0.19$  dpm/g, Figure 1) are in agreement with  $^{231}\text{Pa}_{\text{xs}}$  data from Frank et al. (2000) who report for the same sediment core PS1768-8 at similar core depth (156-181 cm) a decay corrected  $^{231}\text{Pa}_{\text{xs}}$  activity of  $1.37 \pm 0.27$  dpm/g analyzed with alpha spectrometry. Bulk  $^{231}\text{Pa}_{\text{xs}}/^{230}\text{Th}_{\text{xs}}$  ratios ( $0.16\pm 0.04$ ) are within the range of previously published ratios (0.12-0.24) reported for the glacial Southern Ocean on sediment cores just south of the Antarctic polar front (APF) close to our core site by Kumar et al. (1995) and Anderson et al. (1998).

#### 3.2. Beryllium

##### 3.2.1 $^{10}\text{Be}/^{230}\text{Th}$ distribution by particle type

The fast sinking coarse particles  $>20\ \mu\text{m}$  (opal-poor) are characterized by  $^{10}\text{Be}$  concentrations ( $0.50\pm 0.02 - 0.86\pm 0.03 \times 10^9$  at/g, Figure 1, Table A2 in the Appendix) and  $^{10}\text{Be}/^{230}\text{Th}_{\text{xs}}$  ratios ( $0.21\pm 0.04 - 0.33\pm 0.06 \times 10^9$  at/dpm) lower than within all other particle

403 classes. The slowly sinking coarse particles  $>20\ \mu\text{m}$  (opal-rich) reveal  $^{10}\text{Be}$  concentrations  
404  $(0.84\pm 0.03 - 1.33\pm 0.04 \times 10^9\ \text{at/g})$  slightly higher than the fast sinking particles, but their  
405  $^{10}\text{Be}/^{230}\text{Th}_{\text{xs}}$  ratios  $(0.49\pm 0.08 - 0.57\pm 0.10 \times 10^9\ \text{at/dpm})$  are the highest of all. In contrast, the  
406 fine particles  $<20\ \mu\text{m}$  (opal-rich) carry the highest  $^{10}\text{Be}$  concentrations  $(3.03\pm 0.09 - 3.11\pm 0.10$   
407  $\times 10^9\ \text{at/g})$ , but their  $^{10}\text{Be}/^{230}\text{Th}_{\text{xs}}$  ratios  $(0.39\pm 0.07 - 0.45\pm 0.08 \times 10^9\ \text{at/dpm})$  are equal (within  
408 errors) to the slowly sinking classes.  $^{10}\text{Be}/^{230}\text{Th}_{\text{xs}}$  ratios in all particle size classes exceed the  
409 production ratio in seawater  $(0.136\text{-}0.170 \times 10^9\ \text{at/dpm})$ .

410 Within the same core PS1768-8 at similar core depth (156-181 cm) Frank et al. (2000)  
411 analyzed the  $^{10}\text{Be}$  concentration by chemical leaching of the sediment and report a  $^{10}\text{Be}$   
412 concentration of  $1.23\pm 0.04 \times 10^9\ \text{at/g}$ . This is half the concentration of what we measured by  
413 complete acid digestion  $(2.5\pm 0.1 \times 10^9\ \text{at/g})$ , Figure 1). Either a higher  $^{10}\text{Be}$  signal by complete  
414 digestion may derive from a lithogenic  $^{10}\text{Be}$  source or the recovery of authigenic  $^{10}\text{Be}$  from  
415 marine sediments by acid leaching may be incomplete (Bourles et al., 1989). The cause for  
416 the discrepancy of both  $^{10}\text{Be}$  data cannot be clarified here. In the following paragraph  
417 however, the  $^{10}\text{Be}$  sources are discriminated by using the  $^{10}\text{Be}/\text{Be}$  ratio within the particle  
418 fractions.

419

### 420 *3.2.2 Origin of the $^{10}\text{Be}/\text{Be}$ signal*

421

422 It has been shown that dissolved trace metals are trapped within the silica structure of  
423 diatoms so that past metal concentrations in surface waters are recorded by sedimentary opal  
424 tests (Lal et al., 2006). This idea is supported by the observation of  $^{10}\text{Be}$  depletion in surface  
425 waters of the modern Atlantic ACC which is suggested to result from enhanced scavenging by  
426 opal particles in the euphotic zone (Frank et al., 2002). Following this line of argument, our  
427 slowly settling opal-rich 20-63  $\mu\text{m}$  particle fractions of PS1768 and PS1769 (containing 75  
428 and 82 % biogenic opal, Table A3) largely reflect an authigenic surface water derived  $^{10}\text{Be}/\text{Be}$

429 signal (respectively  $4.26 \pm 0.14$  and  $4.10 \pm 0.17 \times 10^{-8}$  at/at, Figure 1). Assuming that  $^{10}\text{Be}/\text{Be}$  is  
430 equal within all opal tests in all size fractions of PS1768 and PS1769 we can calculate the  
431  $^{10}\text{Be}/\text{Be}$  ratios for pure (i.e. 100 %) biogenic opal to be  $5.7 \pm 0.2$  and  $5.0 \pm 0.2 \times 10^{-8}$  at/at  
432 respectively. The fine particle fractions (<20  $\mu\text{m}$ , clay and fine silt) of PS1768 and PS1769  
433 reveal slightly higher  $^{10}\text{Be}/\text{Be}$  ratios ( $5.46 \pm 0.19$  and  $5.54 \pm 0.20 \times 10^{-8}$  at/at, respectively) than  
434 slowly settling opal-rich >20  $\mu\text{m}$  particles, but they contain less biogenic opal (55 % and 58  
435 %, respectively). We, therefore, suspect that a significant portion of  $^{10}\text{Be}/\text{Be}$  must have been  
436 contributed by the lithogenic component of the fine fraction (i.e. clay and fine silt). Based on  
437 the  $^{10}\text{Be}/\text{Be}$  ratios calculated for the pure biogenic opal we can calculate the  $^{10}\text{Be}/\text{Be}$  ratios in  
438 the pure lithogenic fine fraction to be  $5.2 \pm 0.3$  and  $6.3 \pm 0.3 \times 10^{-8}$  at/at. The deep and bottom  
439 water could be a possible source for  $^{10}\text{Be}$  adsorbed onto clay and fine silt. The ratio reported  
440 for the modern deep and bottom water of the circumpolar current is about  $10\text{-}11 \times 10^{-8}$  at/at  
441 (Kusakabe et al., 1987). Regarding the modern oceanography, it has been suggested that only  
442 an advection of  $^{10}\text{Be}$  from the deep Pacific could explain the high  $^{10}\text{Be}$  concentrations in the  
443 deep water of the Atlantic sector of the Southern Ocean (Frank et al., 2002). Furthermore, the  
444 sedimentary clay mineral assemblage of the Eastern South Atlantic sediments indicates a long  
445 distance transport of lithogenic material originating from Patagonia and the Antarctic  
446 Peninsula (Diekmann et al., 1996). Thus we interpret the high  $^{10}\text{Be}$  concentrations found in  
447 the <20  $\mu\text{m}$ -fraction to be partly derived from the adsorption on clay minerals that are  
448 advected by bottom currents from distant sources. However, if  $^{10}\text{Be}/\text{Be}$  was, as it is today,  
449 even higher in the deep and bottom water than measured in our lithogenic fraction then the  
450 lithogenic component may be diluted with a lower  $^{10}\text{Be}/\text{Be}$  ratio deriving from aeolian dust  
451 that may range from 0.1 to  $2 \times 10^{-8}$ , as reported for surface soils (Barg et al., 1997). The  
452 absolute  $^{10}\text{Be}$  contribution to the deep water by aeolian dust is insignificant (Wang et al.,  
453 1996), acting mainly as a diluting agent. Dust fluxes of 1-5  $\text{g}/\text{m}^2/\text{y}$  have been reported from  
454 ODP core 1090 (Martínez-García et al., 2009).

455 Lal et al. (2006) analyzed  $^{10}\text{Be}/\text{Be}$  in cleaned opal samples that were separated from  
456 sediments (5.8 ka - 125 ka) from the ODP core 1093 located very close to our core site. The  
457  $^{10}\text{Be}/\text{Be}$  ratios in these opal tests widely range between 0.19 and  $50 \times 10^{-8}$  at/at and the error  
458 associated with the  $^{10}\text{Be}/\text{Be}$  data can be as high as 20 %. If such large uncertainties are taken  
459 into account for our study, the differences of  $^{10}\text{Be}/\text{Be}$  between particle fractions as discussed  
460 above would be insignificant. Nevertheless, the data of the  $<20 \mu\text{m}$  fraction demonstrate that  
461 lithogenic fines substantially contribute to the  $^{10}\text{Be}/\text{Be}$  signal so that our conclusion is still  
462 valid, i.e. that  $^{10}\text{Be}$  at our study site partly derived from sources other than the ocean surface  
463 water.

464

### 465 *3.3. Influence on isotope ratios by sediment redistribution*

466

467 Comparing the rapid with the slow accumulation site (Figure 1, white and black bars,  
468 respectively) they mostly reveal identical (within  $1\sigma$ ) isotope concentrations and ratios.  
469 Systematic differences between both sites are not observable. Both sites probably receive  
470 particles of the same composition that experience the same water masses, owing to their close  
471 neighborhood and the similar water depth. We conclude that mass accumulation rates and  
472 consequently the total fluxes of Pa, Th and Be may differ widely between two study sites  
473 under contrasting focusing conditions on local scale without affecting their respective isotope  
474 concentrations and ratios.

475 To assess the potential size sorting effect on the isotope signal of the sediments Table  
476 2 provides the percentage of isotopes contributed by each size class in relation to the total  
477 inventories. The fine grained ( $<20 \mu\text{m}$ ) and slowly settling opal-rich particles are the main  
478 contributors to the isotope inventories and therefore they determine the sedimentary isotope  
479 ratios. The size fraction ( $<20 \mu\text{m}$ ) contributes 88-91 % of the total amount of the  
480 radioisotopes in the sediment samples. The differences in contribution by the  $<20 \mu\text{m}$ -fraction

481 are rather small for the three radioisotopes. The opal-rich particle class of size 20-63  $\mu\text{m}$  is  
482 also an important carrier for the three radioisotopes. This class holds more  $^{231}\text{Pa}_{\text{xs}}$  (9-10 %)  
483 than  $^{10}\text{Be}$  (5-7 %) and  $^{230}\text{Th}_{\text{xs}}$  (4-6 %). These differences are essential for the change in  
484 isotope ratios in the case of particle sorting by bottom currents as shown in the following  
485 paragraph.

486 Figure 4 illustrates a simulation of winnowing by progressively removing the fine  
487 sediment component and calculating the resulting radioisotope composition. Two scenarios  
488 for winnowing are shown in Figure 4. The removal of only the finest fraction ( $<20 \mu\text{m}$ ,  
489 dashed line) leads to a slight increase of the  $^{231}\text{Pa}/^{230}\text{Th}$  and the  $^{10}\text{Be}/^{230}\text{Th}$  ratios compared to  
490 the measured bulk composition. The removal of the finest fraction ( $<20 \mu\text{m}$ ) together with the  
491 slowly settling opal-rich particles (solid line) leads to decreasing isotope ratios. Among those  
492 two simulations we expect the second one being the more realistic scenario because the finest  
493 particles and the opal particles are both quite susceptible to resuspension and transport owing  
494 to their hydrodynamic behavior. A substantial removal of the fine and opal-rich particles  
495 (reduction of 70 to 80 % relative to the bulk composition) would reduce the  $^{231}\text{Pa}/^{230}\text{Th}$  ratio  
496 to a value lower than the production ratio (0.093).  $^{10}\text{Be}/^{230}\text{Th}$  ratios would also be affected by  
497 winnowing, but less pronounced than  $^{231}\text{Pa}/^{230}\text{Th}$ . Consequently, strong winnowing at our  
498 study site could fractionate  $^{230}\text{Th}$ ,  $^{231}\text{Pa}$ , and  $^{10}\text{Be}$ .

499 The opposite will happen in case of concentration of the fine and opal-rich particles by  
500 a stronger focusing. However, this stronger focusing could not change significantly the  
501 isotope ratios because the investigated cores are already strongly determined by the  
502 redistributed fines ( $<20 \mu\text{m}$ ) and slowly sinking opal-rich particles making 87-91% of the  
503 sediment (Table 2) so that the sediment setting is much closer to the full-focusing extreme  
504 than to the situation of winnowing. That means that a stronger focusing would hardly change  
505 the isotope ratios.

506           However, regarding the sedimentary setting (strong sediment focusing during glacial  
507 and interglacial; Frank et al., 1996), events of strong winnowing are rather unusual at our  
508 study site. Therefore, an influence of particle sorting on isotope ratios would more probably  
509 occur in regions of strong winnowing, such as, e.g., reported for places south of the  
510 Subantarctic Front between 46°S and 48°S (Frank et al., 1996).

511           We can conclude that moderate variations in fluxes of particulate Th, Be, and Pa by  
512 lateral advection have negligible influence on the sedimentary isotope ratios found at our  
513 study site, and that the isotope ratios reflect particle fluxes on local scale independent of the  
514 mass accumulation rate. This conclusion is only valid if redistribution occurs  
515 syndepositionally and over short distances. In the case of long range particle transport as  
516 already indicated by the  $^{10}\text{Be}$  data any reliable location-specific information on past fluxes of  
517 certain particle types cannot be provided.

518

#### 519 *3.4. Influence of opal content on isotope ratios*

520

521            $^{231}\text{Pa}_{\text{xs}}$ ,  $^{10}\text{Be}$ , and  $^{230}\text{Th}_{\text{xs}}$  concentrations are positively correlated to the specific surface  
522 area, reflecting the adsorptive binding of all three nuclides to the surfaces of particles (Figure  
523 2a). The ratios  $^{231}\text{Pa}_{\text{xs}}/^{230}\text{Th}_{\text{xs}}$  and  $^{10}\text{Be}/^{230}\text{Th}_{\text{xs}}$  are positively correlated with the biogenic opal  
524 content of the particles (Figure 2b) confirming findings of earlier studies (Taguchi et al.,  
525 1989; François et al., 1993; Asmus et al., 1999; Chase et al., 2002; Bradtmiller et al., 2009).  
526 In contrast, the isotope ratios show an anti-correlation to Al (Figure 2b). This is expected as  
527 Al represents the lithogenic component which is anti-correlated to biogenic opal. We  
528 conclude that the capacity of element adsorption is a function of the surface area of the  
529 particle, whereas the ability to fractionate between elements depends on the opal content of  
530 the particle.

531 The consequence is, that in regions where biogenic opal is dominating the particle flux  
532  $^{231}\text{Pa}_{\text{xs}}/^{230}\text{Th}_{\text{xs}}$  cannot reliably indicate neither the ocean ventilation nor the total mass flux.  
533 Thus its use as kinematic proxy and paleoproductivity proxy is limited in those situations.  
534 This confirms the statements of earlier studies (e.g. Walter et al., 1997; Keigwin and Boyle,  
535 2008; Scholten et al., 2008; Lippold et al., 2009). Such effects of particle composition on  
536 sediment  $^{231}\text{Pa}/^{230}\text{Th}$  can be taken into account by analyzing the opal content of the sediment  
537 (Gherardi et al., 2009; Guihou et al., in press). Luo et al (2010), however, demonstrate by a 2-  
538 D model approach, that a change of particle composition in the Southern Ocean could change  
539 the Southern Ocean  $^{231}\text{Pa}$  sink and consequently the sediment  $^{231}\text{Pa}/^{230}\text{Th}$  in the Atlantic  
540 basin.

541 In order to test whether the fractionation by opal content is stronger for either one of  
542 the nuclides  $^{231}\text{Pa}$  or  $^{10}\text{Be}$ , we introduce the distribution ratio  $D(N/\text{Th})$  as a new parameter. As  
543  $D(N/\text{Th})$  is a ratio of percentages, the direct comparison between the Pa-Th- and Be-Th-  
544 fractionation is possible and independent of units. The percentage (i.e. the fraction:bulk ratio)  
545 of the nuclide  $N$  ( $^{231}\text{Pa}$  or  $^{10}\text{Be}$ ) within a certain particle size class is divided by the percentage  
546 of  $^{230}\text{Th}$  within the same particle size class (equation 1),

$$547$$

$$548 \quad D(N/\text{Th}) = [N_{\text{fraction}}/N_{\text{bulk}}] / [\text{Th}_{\text{fraction}}/\text{Th}_{\text{bulk}}], \quad (1)$$

549

550 where  $N$  is the concentration of either  $^{231}\text{Pa}_{\text{xs}}$  or  $^{10}\text{Be}$ , and  $\text{Th}$  is the concentration of  $^{230}\text{Th}_{\text{xs}}$ .  
551 Deviation of  $D(N/\text{Th})$  from 1.0 reflects adsorption intensities of  $N$  different from that of  $\text{Th}$ .  
552  $D(N/\text{Th}) > 1$  indicates preferential adsorption and  $0 < D(N/\text{Th}) < 1$  indicates less adsorption of  $N$   
553 relative to  $\text{Th}$ . The  $D(N/\text{Th})$  ratio is displayed in Figure 3 on a logarithmic scale where bars  
554 are sorted from left to right by increasing opal content. As expected, preferential scavenging  
555 of  $\text{Th}$  relative to  $\text{Pa}$  and  $\text{Be}$  is found in the opal-poor particles ( $D(N/\text{Th}) = 0.2-0.9$ ), whereas the  
556 inverse situation is found within the opal-rich particle classes ( $D(N/\text{Th}) = 1.3-3.3$ ). Within all



557 particle classes,  $D(^{10}\text{Be}/^{230}\text{Th})$  is closer to unity than  $D(^{231}\text{Pa}/^{230}\text{Th})$ . That means the  
558 fractionation between  $^{230}\text{Th}$  and  $^{10}\text{Be}$  is less sensitive to the opal content than the fractionation  
559 between  $^{230}\text{Th}$  and  $^{231}\text{Pa}$ . This is consistent with results of other investigators suggesting that  
560  $^{10}\text{Be}$  scavenging is sensitive to both opal and lithogenic particles fluxes (e.g. Lao et al., 1992;  
561 Frank et al., 2000; Chase et al., 2002), whereas opal is the major phase for Pa scavenging  
562 (Chase et al., 2002; Scholten et al., 2005).

563         The size classes  $<2\ \mu\text{m}$  and  $<20\ \mu\text{m}$  show  $D(^{231}\text{Pa}/^{230}\text{Th})$  values close to unity in spite  
564 of their high opal concentrations (55-70 %). These particle fractions contain the highest  
565 concentrations of both  $^{231}\text{Pa}_{\text{xs}}$  (Figure 1) and  $^{230}\text{Th}_{\text{xs}}$  (Table A1). Assuming the most extreme  
566 case to explain this observation, virtually all  $^{231}\text{Pa}$  could be scavenged by opal particles, and  
567 virtually all  $^{230}\text{Th}$  could be scavenged by clay minerals. The actual contribution of the  
568 individual particle types to total  $^{231}\text{Pa}$  and  $^{230}\text{Th}$ , however, cannot be fully resolved here and  
569 must be addressed in further investigations.

#### 4. CONCLUSIONS

570

571

572           Within various studies the biogenic opal was suggested to be the major influencing  
573 factor for  $^{231}\text{Pa}_{\text{xs}}$  and  $^{10}\text{Be}$  scavenging in the water column. Our data show that  $^{231}\text{Pa}_{\text{xs}}$  and  
574  $^{10}\text{Be}$  remain strongly associated to the opal-rich particles even after burial in the sediment.  
575 The fractionation from  $^{230}\text{Th}_{\text{xs}}$  by opal-rich particles is more pronounced for  $^{231}\text{Pa}_{\text{xs}}$  than for  
576  $^{10}\text{Be}$ . In congruence with previous studies we can conclude that opal fluxes in sediments are  
577 better recorded by  $^{231}\text{Pa}_{\text{xs}}$  than by  $^{10}\text{Be}$ . Our data support the view of Frank et al. (2000) who  
578 conclude from observations on the same sediment core (PS1768-8) that the  $^{10}\text{Be}$  flux rate is  
579 not a suitable tracer for biogenic particle flux in the Southern Ocean. Owing to its sensitivity  
580 to both lithogenic particle flux and biogenic opal flux  $^{10}\text{Be}$  should be used as tracer for total  
581 particle fluxes and its application should be restricted to situations where oceanic particle  
582 composition does not change significantly over time.

583           The particle specific  $^{10}\text{Be}/\text{Be}$  ratios reveal that the opal-rich particles reflect a local  
584  $^{10}\text{Be}$  signal derived from sea surface, whereas the maximum  $^{10}\text{Be}$  concentrations and  $^{10}\text{Be}/\text{Be}$   
585 ratios within the fine particles  $<20\ \mu\text{m}$  point to another  $^{10}\text{Be}$  source, possibly adsorbed to clay,  
586 equilibrated with deep water masses, and advected by bottom currents.

587           Our experiments have shown that biogenic opal fractionates  $^{231}\text{Pa}$  and  $^{230}\text{Th}$ . In  
588 regions of high latitudes where biogenic opal dominates the particle fluxes the scavenging  
589 efficiency of  $^{231}\text{Pa}$  is increased relative to  $^{230}\text{Th}$ . Therefore,  $^{231}\text{Pa}/^{230}\text{Th}$  is not a reliable proxy  
590 for total particle flux in the Southern Ocean. However, based on our data we confirm that  
591  $^{231}\text{Pa}_{\text{xs}}$  is as reasonable tracer for opal fluxes into the Southern Ocean sediments as recently  
592 applied by Anderson et al. (2009) and Bradtmiller et al. (2009).

593           Many studies have applied the  $^{231}\text{Pa}_{\text{xs}}/^{230}\text{Th}_{\text{xs}}$  and  $^{10}\text{Be}/^{230}\text{Th}_{\text{xs}}$  ratios for  
594 paleoceanographic reconstructions on sediments deposited under rapid accumulation, making  
595 the assumption that isotope ratios are not influenced by accumulation rate and sediment

596 transport. Our results partly confirm this assumption, because concentrations and ratios  
597 appear to be insensitive to local variations in the focusing intensity. Based on our data, the  
598 fractionation of  $^{231}\text{Pa}$ ,  $^{10}\text{Be}$ , and  $^{230}\text{Th}$  by transport processes appears unlikely at our Southern  
599 Ocean study site. A definite conclusion, however, cannot be drawn as we do not have data  
600 from a corresponding winnowing site.

601 The simulation of winnowing (Figure 4) shows that particle sorting could change  
602 isotope ratios. An extreme sediment winnowing (removal of 70-80 % of fines) would remove  
603 high  $^{231}\text{Pa}/^{230}\text{Th}$  and  $^{10}\text{Be}/^{230}\text{Th}$  ratios that are associated to the hydrodynamically mobile  
604 opal-rich sediment fraction whereas the corresponding low isotope ratios are left behind  
605 associated to the hydrodynamically stationary sediment fraction.

606 This study shows the potential effect of particle composition and redistribution on  
607 sediment  $^{231}\text{Pa}/^{230}\text{Th}$  which must be taken into account for the reconstructions of the Atlantic  
608 meridional overturning circulation. In case of drift deposits and sediments with high opal  
609 concentrations the use of  $^{231}\text{Pa}/^{230}\text{Th}$  as kinematic proxy should be avoided.

610 The compound-specific information about  $^{231}\text{Pa}_{\text{xs}}/^{230}\text{Th}_{\text{xs}}$  and  $^{10}\text{Be}/^{230}\text{Th}_{\text{xs}}$ , which we  
611 determined here, shows the potential to trace the origin of an isotopic signature better than the  
612 previously accessible bulk isotope ratios. This allows to a certain extent to discriminate  
613 signals of remote origin and local signals from surface waters.

614            *Acknowledgements.* We thank Allan Davidson (NERC CIAF) and Ingrid Stimac  
615 (AWI) for their help in the lab, and Rainer Gersonde for providing the sediment samples. The  
616 funding for this work was provided by a Helmholtz University Young Investigators Group  
617 grant to GM. NERC granted financial support to WG for the AMS analyses at SUERC  
618 (project 9040.1007). The DAAD (project D/08/40703) funded the stay abroad for SK  
619 participating in the <sup>10</sup>Be sample preparation at the NERC CIAF. Comments by S.  
620 Krishnaswami, M. Frank and two anonymous reviewers helped improving the manuscript.

621 References

622

623 Anderson R. F., Bacon M. P. and Brewer P. G. (1983a) Removal of  $^{230}\text{Th}$  and  $^{231}\text{Pa}$  at ocean  
624 margins. *Earth and Planetary Science Letters* **66**, 73-90. doi:10.1016/0012-  
625 821X(83)90127-9

626 Anderson R. F., Bacon M. P. and Brewer P. G. (1983b) Removal of  $^{230}\text{Th}$  and  $^{231}\text{Pa}$  from the  
627 open ocean. *Earth and Planetary Science Letters* **62**, 7-23. doi:10.1016/0012-  
628 821X(83)90067-5

629 Anderson R. F., Lao Y., Broecker W. S., Trumbore S. E., Hofmann H. J. and Wölfli W.  
630 (1990) Boundary Scavenging in the Pacific Ocean - A Comparison of  $^{10}\text{Be}$  and  $^{231}\text{Pa}$ .  
631 *Earth and Planetary Science Letters* **96**, 287-304. doi:10.1016/0012-821X(90)90008-  
632 L

633 Anderson R. F., Fleisher M. Q., Biscaye P. E., Kumar N., Dittrich B., Kubik P. and Suter M.  
634 (1994) Anomalous boundary scavenging in the Middle Atlantic Bight: evidence from  
635  $^{230}\text{Th}$ ,  $^{231}\text{Pa}$ ,  $^{10}\text{Be}$  and  $^{210}\text{Pb}$ . *Deep Sea Research Part II: Topical Studies in*  
636 *Oceanography* **41**, 537-561. doi:10.1016/0967-0645(94)90034-5

637 Anderson R. F., Kumar N., Mortlock R. A., Froelich P. N., Kubik P., Dittrich-Hannen B. and  
638 Suter M. (1998) Late-Quaternary changes in productivity of the Southern Ocean.  
639 *Journal of Marine Systems* **17**, 497-514. doi:10.1016/S0924-7963(98)00060-8

640 Anderson R. F., Ali S., Bradtmiller L. I., Nielsen S. H. H., Fleisher M. Q., Anderson B. E. and  
641 Burckle L. H. (2009) Wind-Driven Upwelling in the Southern Ocean and the  
642 Deglacial Rise in Atmospheric  $\text{CO}_2$ . *Science* **323**, 1443-1448.  
643 doi:10.1126/science.1167441

644 Asmus T., Frank M., Koschmieder C., Frank N., Gersonde R., Kuhn G. and Mangini A.  
645 (1999) Variations of biogenic particle flux in the southern Atlantic section of the

646 Subantarctic Zone during the late Quaternary: Evidence from sedimentary  $^{231}\text{Pa}_{\text{ex}}$  and  
647  $^{230}\text{Th}_{\text{ex}}$ . *Marine Geology* **159**, 63-78. doi:10.1016/S0025-3227(98)00199-6

648 Bacon M. P. (1984) Glacial to Interglacial Changes in Carbonate and Clay Sedimentation in  
649 the Atlantic-Ocean Estimated from Th-230 Measurements. *Isotope Geoscience* **2**, 97-  
650 111.

651 Barg E., Lal D., Pavich M. J., Caffee M. W. and Southon J. R. (1997) Beryllium  
652 geochemistry in soils: evaluation of  $^{10}\text{Be}/^9\text{Be}$  ratios in authigenic minerals as a basis  
653 for age models. *Chemical Geology* **140**, 237-258. doi:10.1016/S0009-2541(97)00051-  
654 X

655 Bourles D. L., Raisbeck G. M. and Yiou F. (1989)  $^{10}\text{Be}$  and  $^9\text{Be}$  in marine sediments and their  
656 potential for dating. *Geochimica et Cosmochimica Acta* **53**, 443-452.  
657 doi:10.1016/0016-7037(89)90395-5

658 Bradtmiller L. I., Anderson R. F., Fleisher M. Q. and Burckle L. H. (2007) Opal burial in the  
659 equatorial Atlantic Ocean over the last 30 ka: Implications for glacial-interglacial  
660 changes in the ocean silicon cycle. *Paleoceanography* **22**, PA4216.  
661 doi:10.1029/2007PA001443

662 Bradtmiller L. I., Anderson R. F., Fleisher M. Q. and Burckle L. H. (2009) Comparing glacial  
663 and Holocene opal fluxes in the Pacific sector of the Southern Ocean.  
664 *Paleoceanography* **24**, PA2214. doi:10.1029/2008PA001693

665 Brunauer S., Emmett P. H. and Teller E. (1938) Adsorption of Gases in Multimolecular  
666 Layers. *Journal of the American Chemical Society* **60**, 309-319.

667 Burke A., Marchal O., Bradtmiller L. I., McManus J. F. and François R. (2011) Application  
668 of an inverse method to interpret  $^{231}\text{Pa}/^{230}\text{Th}$  observations from marine sediments.  
669 *Paleoceanography* **26**, PA1212. doi:10.1029/2010PA002022

670 Chase Z., Anderson R. F., Fleisher M. Q. and Kubik P. W. (2002) The influence of particle  
671 composition and particle flux on scavenging of Th, Pa and Be in the ocean. *Earth and*  
672 *Planetary Science Letters* **204**, 215-229. doi:10.1016/S0012-821X(02)00984-6

673 Chase Z., Anderson R. F., Fleisher M. Q. and Kubik P. W. (2003) Scavenging of  $^{230}\text{Th}$ ,  $^{231}\text{Pa}$   
674 and  $^{10}\text{Be}$  in the Southern Ocean (SW Pacific sector): the importance of particle flux,  
675 particle composition and advection *Deep Sea Research Part II: Topical Studies in*  
676 *Oceanography* **50**, 739-768. doi:10.1016/S0967-0645(02)00593-3

677 Chase Z. and Anderson R. F. (2004) Comment on "On the importance of opal, carbonate, and  
678 lithogenic clays in scavenging and fractionating  $^{230}\text{Th}$ ,  $^{231}\text{Pa}$  and  $^{10}\text{Be}$  in the ocean" by  
679 S. Luo and T.-L. Ku. *Earth and Planetary Science Letters* **220**, 213-222.  
680 doi:10.1016/S0012-821X(04)00028-7

681 Christl M., Mangini A. and Kubik P. W. (2007) Highly resolved Beryllium-10 record from  
682 ODP Site 1089 - A global signal? *Earth and Planetary Science Letters* **257**, 245-258.  
683 doi:10.1016/j.epsl.2007.02.035

684 Christl M., Lippold J., Steinhilber F., Bernsdorff F. and Mangini A. (2010) Reconstruction of  
685 global  $^{10}\text{Be}$  production over the past 250 ka from highly accumulating Atlantic drift  
686 sediments. *Quaternary Science Reviews* **29**, 2663-2672.  
687 doi:10.1016/j.quascirev.2010.06.017

688 Diekmann B., Petschick R., Gingele F. X., Fütterer D. K., Abelmann A., Brathauer U.,  
689 Gersonde R. and Mackensen A. (1996) Clay mineral fluctuations in Late Quaternary  
690 sediments of the southeastern South Atlantic: Implications for past changes of deep  
691 water advection. In: G. Wefer, W. H. Berger, G. Siedler, and D. J. Webb (Eds.), *South*  
692 *Atlantic - Present and Past Circulation*. Springer-Verlag Berlin, Berlin. 621-644

693 Dutay J. C., Lacan F., Roy-Barman M. and Bopp L. (2009) Influence of particle size and type  
694 on  $^{231}\text{Pa}$  and  $^{230}\text{Th}$  simulation with a global coupled biogeochemical-ocean general

695 circulation model: A first approach. *Geochemistry Geophysics Geosystems* **10**,  
696 Q01011. doi:10.1029/2008GC002291

697 Finkel R., Krishnaswami S. and Clark D. L. (1977)  $^{10}\text{Be}$  in Arctic Ocean sediments. *Earth*  
698 *and Planetary Science Letters* **35**, 199-204.

699 François R., Bacon M. P., Altabet M. A. and Labeyrie L. D. (1993) Glacial/Interglacial  
700 Changes in Sediment Rain Rate in the SW Indian Sector of Subantarctic Waters as  
701 Recorded by  $^{230}\text{Th}$ ,  $^{231}\text{Pa}$ , U, and  $\delta^{15}\text{N}$ . *Paleoceanography* **8**, 611-629.  
702 doi:10.1029/93PA00784

703 François R., Frank M., Rutgers van der Loeff M. M. and Bacon M. P. (2004)  $^{230}\text{Th}$   
704 normalization: An essential tool for interpreting sedimentary fluxes during the late  
705 Quaternary *Paleoceanography* **19**, doi:10.1029/2003PA000939.

706 Frank M., Mangini A., Gersonde R., Rutgers van der Loeff M. and Kuhn G. (1996) Late  
707 Quaternary sediment dating and quantification of lateral sediment redistribution  
708 applying  $^{230}\text{Th}_{\text{ex}}$ : a study from the eastern Atlantic sector of the Southern Ocean.  
709 *Geologische Rundschau* **85**, 554-566. doi:10.1007/BF02369010

710 Frank M., Schwarz B., Baumann S., Kubik P. W., Suter M. and Mangini A. (1997) A 200 kyr  
711 record of cosmogenic radionuclide production rate and geomagnetic field intensity  
712 from  $^{10}\text{Be}$  in globally stacked deep-sea sediments. *Earth and Planetary Science*  
713 *Letters* **149**, 121-129. doi:10.1016/S0012-821X(97)00070-8

714 Frank M. (2000) Comparison of cosmogenic radionuclide production and geomagnetic field  
715 intensity over the last 200 000 years. *Phil. Trans R. Soc. Lond. A* **358**, 1089-1107.  
716 doi:10.1098/rsta.2000.0575

717 Frank M., Gersonde R., Rutgers van der Loeff M., Bohrmann G., Nürnberg C. C., Kubik P.,  
718 Suter M. and Mangini A. (2000) Similar glacial and interglacial export bioproductivity  
719 in the Atlantic sector of the Southern Ocean: Multiproxy evidence and implications for  
720 glacial atmospheric  $\text{CO}_2$  *Paleoceanography* **15**, 642-658. doi:10.1029/2000PA000497



721 Frank M., Rutgers van der Loeff M. M., Kubik P. W. and Mangini A. (2002) Quasi-  
722 conservative behaviour of  $^{10}\text{Be}$  in deep waters of the Weddell Sea and the Atlantic  
723 sector of the Antarctic Circumpolar Current. *Earth and Planetary Science Letters* **201**,  
724 171-186. doi:10.1016/S0012-821X(02)00688-X

725 Frank M., Backman J., Jakobsson M., Moran K., O'Regan M., King J., Haley B. A., Kubik P.  
726 W. and Garbe-Schönberg D. (2008) Beryllium isotopes in central Arctic Ocean  
727 sediments over the past 12.3 million years: Stratigraphic and paleoclimatic  
728 implications. *Paleoceanography* **23**, PA1S02. doi:10.1029/2007PA001478

729 Freeman S., Bishop P., Bryant C., Cook G., Dougans D., Ertunc T., Fallick A., Ganeshram R.,  
730 Maden C., Naysmith P., Schnabel C., Scott M., Summerfield M. and Xu S. (2007) The  
731 SUERC AMS laboratory after 3 years. *Nuclear Instruments and Methods in Physics*  
732 *Research Section B: Beam Interactions with Materials and Atoms* **259**, 66-70.  
733 doi:10.1016/j.nimb.2007.01.312

734 Geibert W. and Usbeck R. (2004) Adsorption of thorium and protactinium onto different  
735 particle types: experimental findings. *Geochimica et Cosmochimica Acta* **68**, 1489-  
736 1501. doi:10.1016/j.gca.2003.10.011

737 Geibert W., Rutgers van der Loeff M. M., Usbeck R., Gersonde R., Kuhn G. and Seeberg-  
738 Elverfeldt J. (2005) Quantifying the opal belt in the Atlantic and southeast Pacific  
739 sector of the Southern Ocean by means of  $^{230}\text{Th}$  normalization. *Global*  
740 *Biogeochemical Cycles* **19**, GB4001. doi:10.1029/2005GB002465

741 Gersonde R. and Hempel G. (1990) Die Expedition ANTARKTIS-VIII/3 und VIII/4 mit FS  
742 "Polarstern" 1989. *Berichte zur Polarforschung* **74**, 173 pp.  
743 doi:10013/epic.10074.d001

744 Gherardi J. M., Labeyrie L., Nave S., Francois R., McManus J. F. and Cortijo E. (2009)  
745 Glacial-interglacial circulation changes inferred from  $^{231}\text{Pa}/^{230}\text{Th}$  sedimentary record

746 in the North Atlantic region. *Paleoceanography* **24**, PA2204.  
747 doi:10.1029/2008PA001696

748 Gil I. M., Keigwin L. D. and Abrantes F. G. (2009) Deglacial diatom productivity and surface  
749 ocean properties over the Bermuda Rise, northeast Sargasso Sea. *Paleoceanography*  
750 **24**, PA4101. doi:10.1029/2008PA001729

751 Guihou A., Pichat S., Nave S., Govin A., Labeyrie L., Michel E. and Waelbroeck C. (2010)  
752 Late slowdown of the Atlantic Meridional Overturning Circulation during the Last  
753 Glacial Inception: New constraints from sedimentary ( $^{231}\text{Pa}/^{230}\text{Th}$ ). *Earth and*  
754 *Planetary Science Letters* **289**, 520-529. doi:10.1016/j.epsl.2009.11.045

755 Guihou A., Pichat S., Govin A., Nave S., Michel E., Duplessy J.-C., Telouk P. and Labeyrie  
756 L. (in press) Enhanced Atlantic Meridional Overturning Circulation supports the Last  
757 Glacial Inception. *Quaternary Science Reviews*. doi:10.1016/j.quascirev.2011.03.017

758 Guo L. D., Chen M. and Gueguen C. (2002) Control of Pa/Th ratio by particulate chemical  
759 composition in the ocean. *Geophysical Research Letters* **29**.  
760 doi:10.1029/2002GL015666

761 Hansen R. G. and Ring E. J. (1983) *The Preparation and Certification of a Uranium*  
762 *reference material*. Council for Mineral Technology, Randburg, South Africa.

763 Henderson G. M., Heinze C., Anderson R. F. and Winguth A. M. E. (1999) Global  
764 distribution of the  $^{230}\text{Th}$  flux to ocean sediments constrained by GCM modelling.  
765 *Deep Sea Research Part I: Oceanographic Research Papers* **46**, 1861-1893.  
766 doi:10.1016/S0967-0637(99)00030-8

767 Henderson G. M. and Anderson R. F. (2003) The U-series toolbox for paleoceanography. In:  
768 B. Bourdon, G. M. Henderson, C. C. Lundstrom, and S. P. Turner (Eds.), *Uranium-*  
769 *Series Geochemistry*. Mineralogical Society of America, Washington. 493-531

770 Henderson G. M., Anderson R. F., Adkins J., Andersson P., Boyle E. A., Cutter G., de Baar  
771 H., Eisenhauer A., Frank M., Francois R., Orians K., Gamo T., German C., Jenkins

772 W., Moffett J., Jeandel C., Jickells T., Krishnaswami S., Mackey D., Measures C. I.,  
773 Moore J. K., Oeschies A., Pollard R., van der Loeff M. R. D., Schlitzer R., Sharma M.,  
774 von Damm K., Zhang J. and Masque P. (2007) GEOTRACES - An international study  
775 of the global marine biogeochemical cycles of trace elements and their isotopes.  
776 *Chemie Der Erde-Geochemistry* **67**, 85-131. doi:10.1016/j.chemer.2007.02.001

777 Henken-Mellies W. U., Beer J., Heller F., Hsü K. J., Shen C., Bonani G., Hofmann H. J.,  
778 Suter M. and Wölfli W. (1990)  $^{10}\text{Be}$  and  $^9\text{Be}$  in South Atlantic DSDP Site 519:  
779 Relation to geomagnetic reversals and to sediment composition. *Earth and Planetary*  
780 *Science Letters* **98**, 267-276. doi:10.1016/0012-821X(90)90029-W

781 ISO9277 Determination of the specific surface area of solids by gas adsorption - BET  
782 method.

783 Keigwin L. D. and Boyle E. A. (2008) Did North Atlantic overturning halt 17,000 years ago?  
784 *Paleoceanography* **23**, PA1101. doi:10.1029/2007PA001500

785 Kretschmer S., Geibert W., Rutgers van der Loeff M. M. and Mollenhauer G. (2010) Grain  
786 size effects on  $^{230}\text{Th}_{\text{xs}}$  inventories in opal-rich and carbonate-rich marine sediments.  
787 *Earth and Planetary Science Letters* **294**, 131-142. doi:10.1016/j.epsl.2010.03.021

788 Krishnaswami S. (1976) Authigenic transition elements in Pacific pelagic clays. *Geochimica*  
789 *et Cosmochimica Acta* **40**(4), 425-434. doi:10.1016/0016-7037(76)90007-7

790 Ku T. L., Kusakabe M., Measures C. I., Southon J. R., Cusimano G., Vogel J. S., Nelson D.  
791 E. and Nakaya S. (1990) Beryllium isotope distribution in the western North Atlantic:  
792 a comparison to the Pacific. *Deep Sea Research Part A. Oceanographic Research*  
793 *Papers* **37**, 795-808. doi:10.1016/0198-0149(90)90007-I

794 Kumar N., Gwiazda R., Anderson R. F. and Froelich P. N. (1993)  $^{231}\text{Pa}/^{230}\text{Th}$  ratios in  
795 sediments as a proxy for past changes in Southern Ocean productivity. *Nature* **362**,  
796 45-48. doi:10.1038/362045a0

797 Kumar N., Anderson R. F., Mortlock R. A., Froelich P. N., Kubik P., Dittrich-Hannen B. and  
798 Suter M. (1995) Increased biological productivity and export production in the glacial  
799 Southern Ocean. *Nature* **378**, 675-680. doi:10.1038/378675a0

800 Kusakabe M., Ku T. L., Vogel J., Southon J. R., Nelson D. E. and Richards G. (1982)  $^{10}\text{Be}$   
801 profiles in seawater. *Nature* **299**, 712-714. doi:10.1038/299712a0

802 Kusakabe M., Ku T. L., Southon J. R., Vogel J. S., Nelson D. E., Measures C. I. and Nozaki  
803 Y. (1987) Distribution of  $^{10}\text{Be}$  and  $^9\text{Be}$  in the Pacific Ocean. *Earth and Planetary  
804 Science Letters* **82**, 231-240. doi:10.1016/0012-821X(87)90198-1

805 Lal D. and Peters B. (1967) Cosmic ray produced radioactivity on the Earth. In *Handbuch der  
806 Physik*, Vol. **46** (ed. S. Fluegge and K. Sitte), pp. 551-612. Springer-Verlag.

807 Lal D. (2002) Cosmogenic Radionuclides. In *Encyclopedia of Atmospheric Sciences* (eds. J.  
808 R. Holton, J. A. Curry, and J. A. Pyle), pp. 1891-1900. Academic Press.

809 Lal D., Charles C., Vacher L., Goswami J. N., Jull A. J. T., McHargue L. and Finkel R. C.  
810 (2006) Paleo-ocean chemistry records in marine opal: Implications for fluxes of trace  
811 elements, cosmogenic nuclides ( $^{10}\text{Be}$  and  $^{26}\text{Al}$ ), and biological productivity.  
812 *Geochimica et Cosmochimica Acta* **70**, 3275-3289. doi:10.1016/j.gca.2006.04.004

813 Langmuir D. and Herman J. S. (1980) The mobility of thorium in natural waters at low  
814 temperatures. *Geochimica et Cosmochimica Acta* **44**, 1753-1766. doi:10.1016/0016-  
815 7037(80)90226-4

816 Lao Y., Anderson R. F., Broecker W. S., Trumbore S. E., Hofmann H. J. and Wölfli W.  
817 (1992) Transport and burial rates of  $^{10}\text{Be}$  and  $^{231}\text{Pa}$  in the Pacific Ocean during the  
818 Holocene period. *Earth and Planetary Science Letters* **113**, 173-189.  
819 doi:10.1016/0012-821X(92)90218-K

820 Lao Y., Anderson R. F., Broecker W. S., Hofmann H. J. and Wölfli W. (1993) Particulate  
821 fluxes of  $^{230}\text{Th}$ ,  $^{231}\text{Pa}$ , and  $^{10}\text{Be}$  in the northeastern Pacific Ocean. *Geochimica et  
822 Cosmochimica Acta* **57**, 205-217. doi:10.1016/0016-7037(93)90479-G

- 823 Lippold J., Grützner J., Winter D., Lahaye Y., Mangini A. and Christl M. (2009) Does  
824 sedimentary  $^{231}\text{Pa}/^{230}\text{Th}$  from the Bermuda Rise monitor past Atlantic Meridional  
825 Overturning Circulation? *Geophysical Research Letters* **36**, L12601.  
826 doi:10.1029/2009GL038068
- 827 Luo S. and Ku T.-L. (1999) Oceanic  $^{231}\text{Pa}/^{230}\text{Th}$  ratio influenced by particle composition and  
828 remineralization. *Earth and Planetary Science Letters* **167**, 183-195.  
829 doi:10.1016/S0012-821X(99)00035-7
- 830 Luo S. and Ku T.-L. (2003) Constraints on deep-water formation from the oceanic  
831 distributions of  $^{10}\text{Be}$ . *J. Geophys. Res.* **108**, 3137. doi:10.1029/2002JC001670
- 832 Luo S. and Ku T.-L. (2004a) Reply to Comment on "On the importance of opal, carbonate,  
833 and lithogenic clays in scavenging and fractionating  $^{230}\text{Th}$ ,  $^{231}\text{Pa}$  and  $^{10}\text{Be}$  in the  
834 ocean". *Earth and Planetary Science Letters* **220**, 223-229. doi:10.1016/S0012-  
835 821X(04)00029-9
- 836 Luo S. and Ku T.-L. (2004b) On the importance of opal, carbonate, and lithogenic clays in  
837 scavenging and fractionating  $^{230}\text{Th}$ ,  $^{231}\text{Pa}$  and  $^{10}\text{Be}$  in the ocean. *Earth and Planetary  
838 Science Letters* **220**, 201-211. doi:10.1016/S0012-821X(04)00027-5
- 839 Luo Y., Francois R. and Allen S. E. (2010) Sediment  $^{231}\text{Pa}/^{230}\text{Th}$  as a recorder of the rate of  
840 the Atlantic meridional overturning circulation: insights from a 2-D model. *Ocean  
841 Science* **6**, 381-400. doi:10.5194/os-6-381-2010
- 842 Martínez-García A., Rosell-Melé A., Geibert W., Gersonde R., Masqué P., Gaspari V. and  
843 Barbante C. (2009) Links between iron supply, marine productivity, sea surface  
844 temperature, and  $\text{CO}_2$  over the last 1.1 Ma. *Paleoceanography* **24**, PA1207.  
845 doi:10.1029/2008PA001657
- 846 McCave I. N., Manighetti B. and Robinson S. G. (1995) Sortable Silt and Fine Sediment  
847 Size/Composition Slicing: Parameters for Palaeocurrent Speed and  
848 Palaeoceanography. *Paleoceanography* **10**. doi:10.1029/94PA03039

- 849 McManus J. F., Francois R., Gherardi J. M., Keigwin L. D. and Brown-Leger S. (2004)  
850 Collapse and rapid resumption of Atlantic meridional circulation linked to deglacial  
851 climate changes. *Nature* **428**, 834-837. doi:10.1038/nature02494
- 852 Middleton R., Brown L., Dezfouly-Arjomandy B. and Klein J. (1993) On  $^{10}\text{Be}$  standards and  
853 the half-life of  $^{10}\text{Be}$ . *Nuclear Instruments and Methods in Physics Research Section B:  
854 Beam Interactions with Materials and Atoms* **82**, 399-403. doi:10.1016/0168-  
855 583X(93)95987-G
- 856 Monaghan M. C., Krishnaswami S. and Turekian K. K. (1986) The global-average production  
857 rate of  $^{10}\text{Be}$ . *Earth and Planetary Science Letters* **76**, 279-287. doi:10.1016/0012-  
858 821X(86)90079-8
- 859 Moore R. M. and Hunter K. A. (1985) Thorium adsorption in the ocean: reversibility and  
860 distribution amongst particle sizes. *Geochimica et Cosmochimica Acta* **49**, 2253-2257.  
861 doi:10.1016/0016-7037(85)90225-X
- 862 Moore R. M. and Millward G. E. (1988) The kinetics of reversible Th reactions with marine  
863 particles. *Geochimica et Cosmochimica Acta* **52**, 113-118. doi:10.1016/0016-  
864 7037(88)90060-9
- 865 Morris J. D., Gosse J., Brachfeld S. and Tera F. (2002) Cosmogenic Be-10 and the Solid  
866 Earth: Studies in Geomagnetism, Subduction Zone Processes, and Active Tectonics.  
867 In: E. S. Grew (Ed.), *Beryllium: Mineralogy, Petrology, and Geochemistry*.  
868 Mineralogical Society of America, Washington. 207-270
- 869 Müller P. J. and Schneider R. (1993) An automated leaching method for the determination of  
870 opal in sediments and particulate matter. *Deep Sea Research Part I: Oceanographic  
871 Research Papers* **40**, 425-444. doi:10.1016/0967-0637(93)90140-X
- 872 Negre C., Zahn R., Thomas A. L., Masqué P., Henderson G. M., Martinez-Mendez G., Hall I.  
873 R. and Mas J. L. (2010) Reversed flow of Atlantic deep water during the Last Glacial  
874 Maximum. *Nature* **468**, 84-88. doi:10.1038/nature09508

875 Niven S. E. H. and Moore R. M. (1993) Thorium sorption in seawater suspensions of  
876 aluminium oxide particles. *Geochimica et Cosmochimica Acta* **57**, 2169-2179.  
877 doi:10.1016/0016-7037(93)90558-E

878 Pichat S., Sims K. W. W., François R., McManus J. F., Brown Leger S. and Albarède F.  
879 (2004) Lower export production during glacial periods in the equatorial Pacific  
880 derived from  $(^{231}\text{Pa}/^{230}\text{Th})_{\text{xs},0}$  measurements in deep-sea sediments. *Paleoceanography*  
881 **19**, PA4023. doi:10.1029/2003PA000994

882 Robinson L. F., Belshaw N. S. and Henderson G. M. (2004) U and Th concentrations and  
883 isotope ratios in modern carbonates and waters from the Bahamas. *Geochimica et*  
884 *Cosmochimica Acta* **68**, 1777-1789. doi:10.1016/j.gca.2003.10.005

885 Robinson L. F., Noble T. L. and McManus J. F. (2008) Measurement of adsorbed and total  
886  $^{232}\text{Th}/^{230}\text{Th}$  ratios from marine sediments. *Chemical Geology* **252**, 169-179.  
887 doi:10.1016/j.chemgeo.2008.02.015

888 Roy-Barman M., Jeandel C., Souhaut M., Rutgers van der Loeff M., Voegelé I., Leblond N. and  
889 Freydier R. (2005) The influence of particle composition on thorium scavenging in the  
890 NE Atlantic ocean (POMME experiment). *Earth and Planetary Science Letters* **240**,  
891 681-693. doi:10.1016/j.epsl.2005.09.059

892 Roy-Barman M., Lemaître C., Ayrault S., Jeandel C., Souhaut M. and Miquel J. C. (2009)  
893 The influence of particle composition on Thorium scavenging in the Mediterranean  
894 Sea. *Earth and Planetary Science Letters* **286**, 526-534.  
895 doi:10.1016/j.epsl.2009.07.018

896 Rutgers van der Loeff M. M. and Berger G. W. (1993) Scavenging of  $^{230}\text{Th}$  and  $^{231}\text{Pa}$  near the  
897 antarctic polar front in the South Atlantic. *Deep Sea Research Part I: Oceanographic*  
898 *Research Papers* **40**, 339-357. doi:10.1016/0967-0637(93)90007-P

899 Scholten J. C., Fietzke J., Vogler S., Rutgers van der Loeff M. M., Mangini A., Koeve W.,  
900 Waniek J., Stoffers P., Antia A. and Kuss J. (2001) Trapping efficiencies of sediment

901 traps from the deep Eastern North Atlantic:: The  $^{230}\text{Th}$  calibration. *Deep Sea Research*  
902 *Part II: Topical Studies in Oceanography* **48**, 2383-2408. doi:10.1016/S0967-  
903 0645(00)00176-4

904 Scholten J. C., Fietzke J., Mangini A., Stoffers P., Rixen T., Gaye-Haake B., Blanz T.,  
905 Ramaswamy V., Sirocko F., Schulz H. and Ittekkot V. (2005) Radionuclide fluxes in  
906 the Arabian Sea: the role of particle composition. *Earth and Planetary Science Letters*  
907 **230**, 319-337. doi:10.1016/j.epsl.2004.11.003

908 Scholten J. C., Fietzke J., Mangini A., Garbe-Schönberg C. D., Eisenhauer A., Schneider R.  
909 and Stoffers P. (2008) Advection and scavenging: Effects on  $^{230}\text{Th}$  and  $^{231}\text{Pa}$   
910 distribution off Southwest Africa. *Earth and Planetary Science Letters* **271**, 159-169.  
911 doi:10.1016/j.epsl.2008.03.060

912 Siddall M., Henderson G. M., Edwards N. R., Frank M., Müller S. A., Stocker T. F. and Joos  
913 F. (2005)  $^{231}\text{Pa} / ^{230}\text{Th}$  fractionation by ocean transport, biogenic particle flux and  
914 particle type. *Earth and Planetary Science Letters* **237**, 135-155.  
915 doi:10.1016/j.epsl.2005.05.031

916 Suman D. O. and Bacon M. P. (1989) Variations in Holocene sedimentation in the North  
917 American Basin determined from  $^{230}\text{Th}$  measurements. *Deep Sea Research Part A.*  
918 *Oceanographic Research Papers* **36**, 869-878. doi:10.1016/0198-0149(89)90033-2

919 Taguchi K., Harada K. and Tsunogai S. (1989) Particulate removal of  $^{230}\text{Th}$  and  $^{231}\text{Pa}$  in the  
920 biologically productive northern North Pacific. *Earth and Planetary Science Letters*  
921 **93**, 223-232. doi:10.1016/0012-821X(89)90070-8

922 Walter H. J., Rutgers van der Loeff M. M. and Hoeltzen H. (1997) Enhanced scavenging of  
923  $^{231}\text{Pa}$  relative to  $^{230}\text{Th}$  in the South Atlantic south of the Polar Front: Implications for  
924 the use of the  $^{231}\text{Pa}/^{230}\text{Th}$  ratio as a paleoproductivity proxy. *Earth and Planetary*  
925 *Science Letters* **149**, 85-100. doi:10.1016/S0012-821X(97)00068-X



- 926 Wang L., Ku T. L., Luo S., Southon J. R. and Kusakabe M. (1996)  $^{26}\text{Al}$ - $^{10}\text{Be}$  systematics in  
927 deep-sea sediments. *Geochimica et Cosmochimica Acta* **60**, 109-119.  
928 doi:10.1016/0016-7037(95)00379-7
- 929 Xu S., Dougans A. B., Freeman S. P. H. T., Schnabel C. and Wilcken K. M. (2010) Improved  
930  $^{10}\text{Be}$  and  $^{26}\text{Al}$ -AMS with a 5 MV spectrometer. *Nuclear Instruments and Methods in*  
931 *Physics Research Section B: Beam Interactions with Materials and Atoms* **268**, 736-  
932 738. doi:10.1016/j.nimb.2009.10.018
- 933 Yang H.-S., Nozaki Y., Sakai H. and Masuda A. (1986) The distribution of  $^{230}\text{Th}$  and  $^{231}\text{Pa}$  in  
934 the deep-sea surface sediments of the Pacific Ocean. *Geochimica et Cosmochimica*  
935 *Acta* **50**, 81-89. doi:10.1016/0016-7037(86)90050-5
- 936 Yu E.-F., Francois R. and Bacon M. P. (1996) Similar rates of modern and last-glacial ocean  
937 thermohaline circulation inferred from radiochemical data. *Nature* **379**, 689-694.  
938 doi:10.1038/379689a0

939 **Tables**

940

941 Table 1: Sieving recoveries and leaching loss of  $^{230}\text{Th}$ ,  $^{231}\text{Pa}$  and  $^{10}\text{Be}$  after the size  
 942 fractionation of the sediment samples. The leaching loss is the amount of  $^{230}\text{Th}$ ,  $^{231}\text{Pa}$  and  
 943  $^{10}\text{Be}$  that was lost by desorption and/or dissolution during sieving/settling and remained in the  
 944 supernatant water, expressed as the percentage of the total initial amount.

samples	Sediment sieved [g]	$^{230}\text{Th}$ in sediment [dpm/g]	Recovery of	seawater used as sieving fluid [kg]	$^{230}\text{Th}$ in supernatant [dpm/kg]	$^{230}\text{Th}$ leached from sediment [dpm]	$^{230}\text{Th}$ lost to
			$^{230}\text{Th}$ after sieving [%]				supernatant in % of total $^{230}\text{Th}$ [%]
PS1768-8	7.7	6.45	87	22.49	0.05332	1.191	2.4
PS1769-1	7.9	6.09	90	19.10	0.05568	1.056	2.2
“unused” seawater				21.69	0.00037		

samples	Sediment sieved [g]	$^{231}\text{Pa}$ in sediment [dpm/g]	Recovery of	seawater used as sieving fluid [kg]	$^{231}\text{Pa}$ in supernatant [dpm/kg]	$^{231}\text{Pa}$ leached from sediment [dpm]	$^{231}\text{Pa}$ lost to
			$^{231}\text{Pa}$ after sieving [%]				supernatant in % of total $^{231}\text{Pa}$ [%]
PS1768-8	7.7	0.83	110	22.49	0.00181	0.032	0.5
PS1769-1	7.9	0.80	109	19.10	0.00169	0.025	0.4
“unused” seawater				21.69	0.00036		

samples	AMS ID	Sediment sieved [g]	$^{10}\text{Be}$ in sediment [at/g]	Recovery of	seawater used as sieving fluid [kg]	$^{10}\text{Be}$ in supernatant [at/kg]	$^{10}\text{Be}$ leached from sediment [at]	$^{10}\text{Be}$ lost to
				$^{10}\text{Be}$ after sieving [%]				supernatant in % of total $^{10}\text{Be}$ [%]
PS1768-8	b2692	14.4	2.54E+09	103	11.31	1.88E+07	2.09E+08	0.6
PS1769-1	b2832	18.6	2.24E+09	104	15.40	1.93E+07	2.92E+08	0.7
“unused” seawater 1	b2693				11.53	3.12E+05		
“unused” seawater 2	b2694				15.51	2.50E+05		

945

946 Table 2: Percentage contribution by particle size classes. Each size class contributes a certain  
 947 fraction to the total flux of opal and particulate  $^{230}\text{Th}_{\text{xs}}$ ,  $^{231}\text{Pa}_{\text{xs}}$ ,  $^{10}\text{Be}$  and Be. Expressed in  
 948 percentage, the comparison between parameters is possible and the potential influence of  
 949 particle size sorting on isotope ratios can be assessed.

particle size class [ $\mu\text{m}$ ]	settling velocity	wt-% size-fraction	percentage contribution [%] to total inventory				
			opal	$^{230}\text{Th}_{\text{xs}}$	$^{231}\text{Pa}_{\text{xs}}$	$^{10}\text{Be}$	Be
sediment core PS1768-8							
<20		76.4	77.1	90.5	88.6	90	83.3
20-63	slow	14.7	20.3	5.9	9.3	7.4	8.8
>63	slow	2.8	1.9	1.1	1.6	1.2	1.9
20-63	fast	2.7	0.5	1.4	0.3	0.7	2.8
>63	fast	3.5	0.1	1.1	0.2	0.7	3.2
sediment core PS1769-1							
<20		72.5	74.7	90.6	87.7	90.4	81.6
20-63	slow	14.9	21.8	4.2	10	5.2	6.3
>63	slow	3	2.1	1	1.4	1.4	1.8
20-63	fast	2.6	0.8	1.8	0.4	0.9	3.8
>63	fast	7	0.6	2.5	0.5	2	6.5

950

951 fast = particles of high specific density which were isolated by their rapid settling velocity in  
 952 seawater (mainly ice rafted debris)

953 slow = particles of low specific density which were isolated by their slow settling velocity in  
 954 seawater (mainly diatoms)

955 **Appendix**

956

957 Table A1: Particle size specific activities of  $^{231}\text{Pa}$  and  $^{230}\text{Th}$  in two sediment samples. The size  
 958 classes  $>20\ \mu\text{m}$  are split in two particle types by their settling velocity (fast and slow) in  
 959 seawater. Data on  $x_s^{230}\text{Th}_0$  are from Kretschmer et al. (2010). The distribution ratio  $D(\text{Pa}/\text{Th})$   
 960 expresses the particle specific distribution of  $x_s^{231}\text{Pa}_0$  relative to the particle specific  
 961 distribution of  $x_s^{230}\text{Th}_0$  (for explanation see text). Excess  $^{231}\text{Pa}_0$  and  $^{230}\text{Th}_0$  activities are decay  
 962 corrected to the time of deposition at 16 ka. The uncertainty is given as  $1\sigma$ . AR = activity  
 963 ratio.

size class	settle velocity	$^{230}\text{Th}$	$x_s^{230}\text{Th}_0$	$^{231}\text{Pa}$	$x_s^{231}\text{Pa}_0$	$x_s\text{Pa}_0/\text{Th}_0$	$D(\text{Pa}/\text{Th})$
[ $\mu\text{m}$ ]		[dpm $\text{g}^{-1}$ ]			[AR]		
sediment core PS1768-8							
bulk		$6.45 \pm 0.12$	$6.68 \pm 1.13$	$0.83 \pm 0.03$	$1.10 \pm 0.19$	$0.16 \pm 0.04$	
<2		$11.91 \pm 0.20$	$12.81 \pm 2.16$	$1.20 \pm 0.01$	$1.59 \pm 0.27$	$0.12 \pm 0.03$	$0.75 \pm 0.25$
2-20		$1.30 \pm 0.03$	$1.23 \pm 0.21$	$0.49 \pm 0.01$	$0.67 \pm 0.11$	$0.54 \pm 0.13$	$3.31 \pm 1.11$
<20		$6.58 \pm 0.11$	$6.94 \pm 1.17$	$1.05 \pm 0.02$	$1.40 \pm 0.24$	$0.20 \pm 0.05$	$1.23 \pm 0.41$
20-63	fast	$2.94 \pm 0.06$	$3.12 \pm 0.53$	$0.12 \pm 0.01$	$0.14 \pm 0.03$	$0.05 \pm 0.01$	$0.27 \pm 0.10$
63-125	fast	$2.50 \pm 0.05$	$2.68 \pm 0.45$	$0.04 \pm 0.00$	$0.03 \pm 0.01$	$0.01 \pm 0.00$	$0.07 \pm 0.03$
>125	fast	$1.39 \pm 0.03$	$1.45 \pm 0.25$	$0.06 \pm 0.00$	$0.08 \pm 0.01$	$0.05 \pm 0.01$	$0.34 \pm 0.11$
>63	fast	$1.75 \pm 0.04$	$1.84 \pm 0.31$	$0.05 \pm 0.00$	$0.06 \pm 0.01$	$0.03 \pm 0.01$	$0.20 \pm 0.07$
20-63	slow	$2.20 \pm 0.04$	$2.34 \pm 0.39$	$0.56 \pm 0.01$	$0.77 \pm 0.13$	$0.33 \pm 0.08$	$2.00 \pm 0.67$
63-125	slow	$2.01 \pm 0.04$	$2.13 \pm 0.36$	$0.53 \pm 0.01$	$0.72 \pm 0.12$	$0.34 \pm 0.08$	$2.05 \pm 0.70$
>125	slow	$3.83 \pm 0.08$	$4.19 \pm 0.71$	$0.35 \pm 0.01$	$0.46 \pm 0.08$	$0.11 \pm 0.03$	$0.67 \pm 0.23$
>63	slow	$2.12 \pm 0.04$	$2.26 \pm 0.38$	$0.52 \pm 0.01$	$0.71 \pm 0.12$	$0.31 \pm 0.08$	$1.91 \pm 0.65$
sediment core PS1769-1							
bulk		$6.09 \pm 0.10$	$6.67 \pm 1.13$	$0.80 \pm 0.02$	$1.10 \pm 0.19$	$0.16 \pm 0.04$	
<2		$11.52 \pm 0.19$	$12.73 \pm 2.15$	$1.38 \pm 0.03$	$1.89 \pm 0.32$	$0.15 \pm 0.04$	$0.90 \pm 0.31$
2-20		$2.03 \pm 0.04$	$2.14 \pm 0.36$	$0.50 \pm 0.01$	$0.68 \pm 0.11$	$0.32 \pm 0.08$	$1.93 \pm 0.65$
<20		$7.02 \pm 0.13$	$7.69 \pm 1.30$	$1.06 \pm 0.05$	$1.45 \pm 0.25$	$0.19 \pm 0.05$	$1.14 \pm 0.39$
20-63	fast	$3.91 \pm 0.07$	$4.16 \pm 0.70$	$0.15 \pm 0.01$	$0.19 \pm 0.03$	$0.05 \pm 0.01$	$0.28 \pm 0.10$
63-125	fast	$2.31 \pm 0.06$	$2.46 \pm 0.42$	$0.05 \pm 0.00$	$0.06 \pm 0.01$	$0.02 \pm 0.01$	$0.15 \pm 0.05$
>125	fast	$1.90 \pm 0.04$	$2.03 \pm 0.34$	$0.07 \pm 0.01$	$0.09 \pm 0.02$	$0.04 \pm 0.01$	$0.27 \pm 0.10$
>63	fast	$2.01 \pm 0.04$	$2.15 \pm 0.36$	$0.06 \pm 0.01$	$0.08 \pm 0.02$	$0.04 \pm 0.01$	$0.23 \pm 0.08$
20-63	slow	$1.59 \pm 0.03$	$1.74 \pm 0.29$	$0.58 \pm 0.02$	$0.81 \pm 0.14$	$0.46 \pm 0.11$	$2.82 \pm 0.96$
63-125	slow	$1.81 \pm 0.03$	$2.00 \pm 0.34$	$0.41 \pm 0.01$	$0.57 \pm 0.10$	$0.28 \pm 0.07$	$1.73 \pm 0.59$
>125	slow	$3.41 \pm 0.07$	$3.79 \pm 0.64$	$0.55 \pm 0.04$	$0.74 \pm 0.13$	$0.20 \pm 0.05$	$1.18 \pm 0.41$
>63	slow	$2.06 \pm 0.04$	$2.28 \pm 0.38$	$0.43 \pm 0.02$	$0.60 \pm 0.10$	$0.26 \pm 0.06$	$1.60 \pm 0.54$

964

965 fast = particles of high specific density which were isolated by their rapid settling velocity in  
 966 seawater (mainly ice rafted debris)

967 slow = particles of low specific density which were isolated by their slow settling velocity in  
 968 seawater (mainly diatoms)

969 Table A2: Particle size specific concentrations and ratios of  $^{10}\text{Be}$ , Be and excess  $^{230}\text{Th}$  in two  
970 sediment samples. The size classes  $>20\ \mu\text{m}$  are split in two particle types by their settling  
971 velocity (fast and slow) in seawater. Data on  $x_s^{230}\text{Th}_0$  are from Kretschmer et al. (2010). The  
972 distribution ratio  $D(\text{Be}/\text{Th})$  expresses the particle specific distribution of  $^{10}\text{Be}$  relative to the  
973 particle specific distribution of  $x_s^{230}\text{Th}_0$  (for explanation see text).  $^{10}\text{Be}$  concentrations and  
974  $x_s^{230}\text{Th}_0$  activities are decay corrected to the time of deposition at 16 ka. The uncertainty is  
975 given as  $1\sigma$ .

AMS ID	size class	settle veloc.	$x_s^{230}\text{Th}_0$	$^{10}\text{Be}$	Be	$^{10}\text{Be}/\text{Be}$	$^{10}\text{Be}/x_s^{230}\text{Th}_0$	$D(\text{Be}/\text{Th})$
	[ $\mu\text{m}$ ]		[dpm $\text{g}^{-1}$ ]	[ $10^9\ \text{at}\ \text{g}^{-1}$ ]	[ $\mu\text{g}\ \text{g}^{-1}$ ]	[ $10^{-8}\ \text{at}\ \text{at}^{-1}$ ]	[ $10^9\ \text{at}\ \text{dpm}^{-1}$ ]	
sediment core PS1768-8								
b2690	bulk		$6.45 \pm 0.12$	$2.56 \pm 0.08$	$0.83 \pm 0.02$	$4.61 \pm 0.17$	$0.38 \pm 0.07$	
b2688	$<20$		$6.58 \pm 0.11$	$3.11 \pm 0.10$	$0.85 \pm 0.01$	$5.46 \pm 0.19$	$0.45 \pm 0.08$	$1.17 \pm 0.28$
b2655	20-63	fast	$2.94 \pm 0.06$	$0.69 \pm 0.02$	$0.81 \pm 0.00$	$1.26 \pm 0.04$	$0.22 \pm 0.04$	$0.58 \pm 0.14$
b2659	$>63$	fast	$1.75 \pm 0.04$	$0.50 \pm 0.02$	$0.72 \pm 0.01$	$1.04 \pm 0.03$	$0.27 \pm 0.05$	$0.71 \pm 0.17$
b2689	20-63	slow	$2.20 \pm 0.04$	$1.33 \pm 0.04$	$0.47 \pm 0.01$	$4.26 \pm 0.14$	$0.57 \pm 0.10$	$1.48 \pm 0.36$
b2658	$>63$	slow	$2.12 \pm 0.04$	$1.15 \pm 0.04$	$0.54 \pm 0.01$	$3.20 \pm 0.12$	$0.51 \pm 0.09$	$1.33 \pm 0.32$
sediment core PS1769-1								
b2660	bulk		$6.09 \pm 0.10$	$2.26 \pm 0.07$	$0.81 \pm 0.01$	$4.16 \pm 0.14$	$0.34 \pm 0.06$	
b2661	$<20$		$7.02 \pm 0.13$	$3.03 \pm 0.09$	$0.82 \pm 0.02$	$5.54 \pm 0.20$	$0.39 \pm 0.07$	$1.16 \pm 0.28$
b2663	20-63	fast	$3.91 \pm 0.07$	$0.86 \pm 0.03$	$1.05 \pm 0.02$	$1.23 \pm 0.04$	$0.21 \pm 0.04$	$0.61 \pm 0.15$
b2664	$>63$	fast	$2.01 \pm 0.04$	$0.70 \pm 0.02$	$0.68 \pm 0.01$	$1.55 \pm 0.05$	$0.33 \pm 0.06$	$0.96 \pm 0.23$
b2662	20-63	slow	$1.59 \pm 0.03$	$0.84 \pm 0.03$	$0.31 \pm 0.01$	$4.10 \pm 0.17$	$0.49 \pm 0.08$	$1.42 \pm 0.35$
b2665	$>63$	slow	$2.06 \pm 0.04$	$1.14 \pm 0.03$	$0.43 \pm 0.01$	$3.91 \pm 0.15$	$0.50 \pm 0.08$	$1.48 \pm 0.36$

976

977 fast = particles of high specific density which were isolated by their rapid settling velocity in  
978 seawater (mainly ice rafted debris)

979 slow = particles of low specific density which were isolated by their slow settling velocity in  
980 seawater (mainly diatoms)

981 Table A3: Particle size specific  $^{232}\text{Th}$ , Aluminum (Al), biogenic opal, and specific surface  
 982 area (SSA) in two sediment samples. The size classes  $>20\ \mu\text{m}$  are split in two particle types  
 983 by their settling velocity (fast and slow) in seawater. Data are from Kretschmer et al. (2010).  
 984 The uncertainty is given as  $1\sigma$ .

size class	settle velocity	$^{232}\text{Th}$	Al	opal	SSA
[ $\mu\text{m}$ ]		[dpm $\text{g}^{-1}$ ]	[%]	[%]	[ $\text{m}^2\ \text{g}^{-1}$ ]
sediment core PS1768-8					
bulk		0.522 $\pm$ 0.009	2.03 $\pm$ 0.03	54.8	
<2		0.842 $\pm$ 0.014	2.37 $\pm$ 0.03	67.7	
2-20		0.256 $\pm$ 0.004	1.38 $\pm$ 0.02	75.6	
<20		0.538 $\pm$ 0.009	2.05 $\pm$ 0.03	54.7	
20-63	fast	0.306 $\pm$ 0.005	5.81 $\pm$ 0.11	14.8	
63-125	fast	0.244 $\pm$ 0.004	7.30 $\pm$ 0.18		
>125	fast	0.181 $\pm$ 0.004	6.17 $\pm$ 0.08	3.4	
>63	fast	0.201 $\pm$ 0.004	6.53 $\pm$ 0.12		
20-63	slow	0.138 $\pm$ 0.002	0.57 $\pm$ 0.02	74.9	
63-125	slow	0.106 $\pm$ 0.002	0.42 $\pm$ 0.01	76.0	
>125	slow	0.222 $\pm$ 0.005	0.95 $\pm$ 0.01		
>63	slow	0.113 $\pm$ 0.002	0.45 $\pm$ 0.01		
sediment core PS1769-1					
bulk		0.461 $\pm$ 0.008	1.97 $\pm$ 0.03	59.8	19.2
<2		0.756 $\pm$ 0.012	2.31 $\pm$ 0.03	61.0	56.5
2-20		0.239 $\pm$ 0.004	1.17 $\pm$ 0.01	79.6	13.0
<20		0.528 $\pm$ 0.007	1.75 $\pm$ 0.02	57.7	33.3
20-63	fast	0.507 $\pm$ 0.008	5.65 $\pm$ 0.11	17.5	2.7
63-125	fast	0.295 $\pm$ 0.006	6.96 $\pm$ 0.08	5.0	1.6
>125	fast	0.231 $\pm$ 0.004	6.86 $\pm$ 0.03	4.2	3.3
>63	fast	0.248 $\pm$ 0.004	6.89 $\pm$ 0.05	4.4	2.2
20-63	slow	0.091 $\pm$ 0.002	0.35 $\pm$ 0.00	81.9	11.2
63-125	slow	0.096 $\pm$ 0.002	0.48 $\pm$ 0.00	79.1	9.5
>125	slow	0.210 $\pm$ 0.004	0.78 $\pm$ 0.00		
>63	slow	0.113 $\pm$ 0.002	0.53 $\pm$ 0.00		

985  
 986 fast = particles of high specific density which were isolated by their rapid settling velocity in  
 987 seawater (mainly ice rafted debris)  
 988 slow = particles of low specific density which were isolated by their slow settling velocity in  
 989 seawater (mainly diatoms)

990 **Figure captions**

991

992 Figure 1: Concentrations of  $^{231}\text{Pa}_{\text{xs}}$  and  $^{10}\text{Be}$  and isotope ratios of excess  $^{231}\text{Pa}/^{230}\text{Th}$  and  
993  $^{10}\text{Be}/^{230}\text{Th}$  in two sediment samples distributed by particle classes [ $\mu\text{m}$ ]. The bulk sediment  
994 was split into size-classes by sieving. Subsequently, particles of different specific densities in  
995 size-classes  $>20 \mu\text{m}$  were split by their settling velocity in seawater into a rapidly settling  
996 fraction (higher density, mainly ice-rafted debris of lithogenic source) and a slowly settling  
997 fraction (lower density, mainly biogenic opal of diatoms). The error bars display the  
998 analytical uncertainty of  $1\sigma$ . Grey horizontal lines indicate the production ratio of  
999  $^{231}\text{Pa}_{\text{xs}}/^{230}\text{Th}_{\text{xs}}$  (0.093) and a range of the production ratio of  $^{10}\text{Be}/^{230}\text{Th}_{\text{xs}}$  ( $0.136\text{-}0.170 \times 10^9$  at  
1000  $\text{dpm}^{-1}$ ). This range is based on  $^{230}\text{Th}$  production at 3300 m water depth and a global average  
1001 production of  $^{10}\text{Be}$  at about 16 ka BP between  $1.2$  and  $1.5 \times 10^6$  at  $\text{cm}^2 \text{yr}^{-1}$  derived from  
1002 Christl et al. (2007) and Frank et al. (1997).

1003

1004 Figure 2: **(a)**  $^{231}\text{Pa}_{\text{xs}}$  and  $^{230}\text{Th}_{\text{xs}}$  specific activities [ $\text{dpm g}^{-1}$ ] and  $^{10}\text{Be}$  concentrations [ $10^9$  at  $\text{g}^{-1}$ ]  
1005  $^1$ ] in particle classes (error bar =  $1\sigma$ ) are plotted against the specific surface area (ssa) [ $\text{m}^2 \text{g}^{-1}$ ]  
1006 of the particles. **(b)**  $^{231}\text{Pa}_{\text{xs}}/^{230}\text{Th}_{\text{xs}}$  [activity ratio] and  $^{10}\text{Be}/^{230}\text{Th}_{\text{xs}}$  [ $10^9$  at  $\text{dpm}^{-1}$ ] in particle  
1007 classes are plotted against biogenic opal [%], aluminum concentration [%] and  $^{232}\text{Th}$  specific  
1008 activity [ $\text{dpm g}^{-1}$ ] (error bar =  $1\sigma$ ). Data and methods on specific surface area, biogenic opal  
1009 content and Al concentrations are reported by Kretschmer et al. (2010).

1010

1011 Figure 3: The distribution ratio  $D(N/\text{Th})$  (see text for definition) is calculated for each particle  
1012 fraction. Values of  $D$  are plotted on a logarithmic scale, where  $0 < D < 1$  indicates a  
1013 fractionation that favors  $^{230}\text{Th}$  over the radionuclide  $N$  ( $^{231}\text{Pa}$  or  $^{10}\text{Be}$ ), and  $D > 1$  indicates a  
1014 fractionation that favors the radionuclide  $N$  ( $^{231}\text{Pa}$  or  $^{10}\text{Be}$ ) over  $^{230}\text{Th}$ . The samples are

1015 ordered on the x-axis with increasing biogenic opal content from left to right. Numbers above  
1016 the bars indicate the particle sizes [ $\mu\text{m}$ ].

1017

1018 Figure 4: Simulating the effect of winnowing on the isotope ratios **(a)**  $^{231}\text{Pa}_{\text{xs}}/^{230}\text{Th}_{\text{xs}}$  and **(b)**  
1019  $^{10}\text{Be}/^{230}\text{Th}_{\text{xs}}$  for the sediment sample PS1768-8. Starting with the bulk composition, the fine  
1020 fraction is progressively removed and the resulting composition is calculated by using grain  
1021 size and isotopic concentration data (Table 2). The resulting isotope ratio depends on the type  
1022 of particles being removed: removal of only fine particles  $<20 \mu\text{m}$  (dashed line) leads to an  
1023 increase of isotope ratios, while the combined removal of  $<20 \mu\text{m}$ -particles and opal-rich  
1024 particles (solid line) leads to a decrease of isotope ratios.



Figure 1

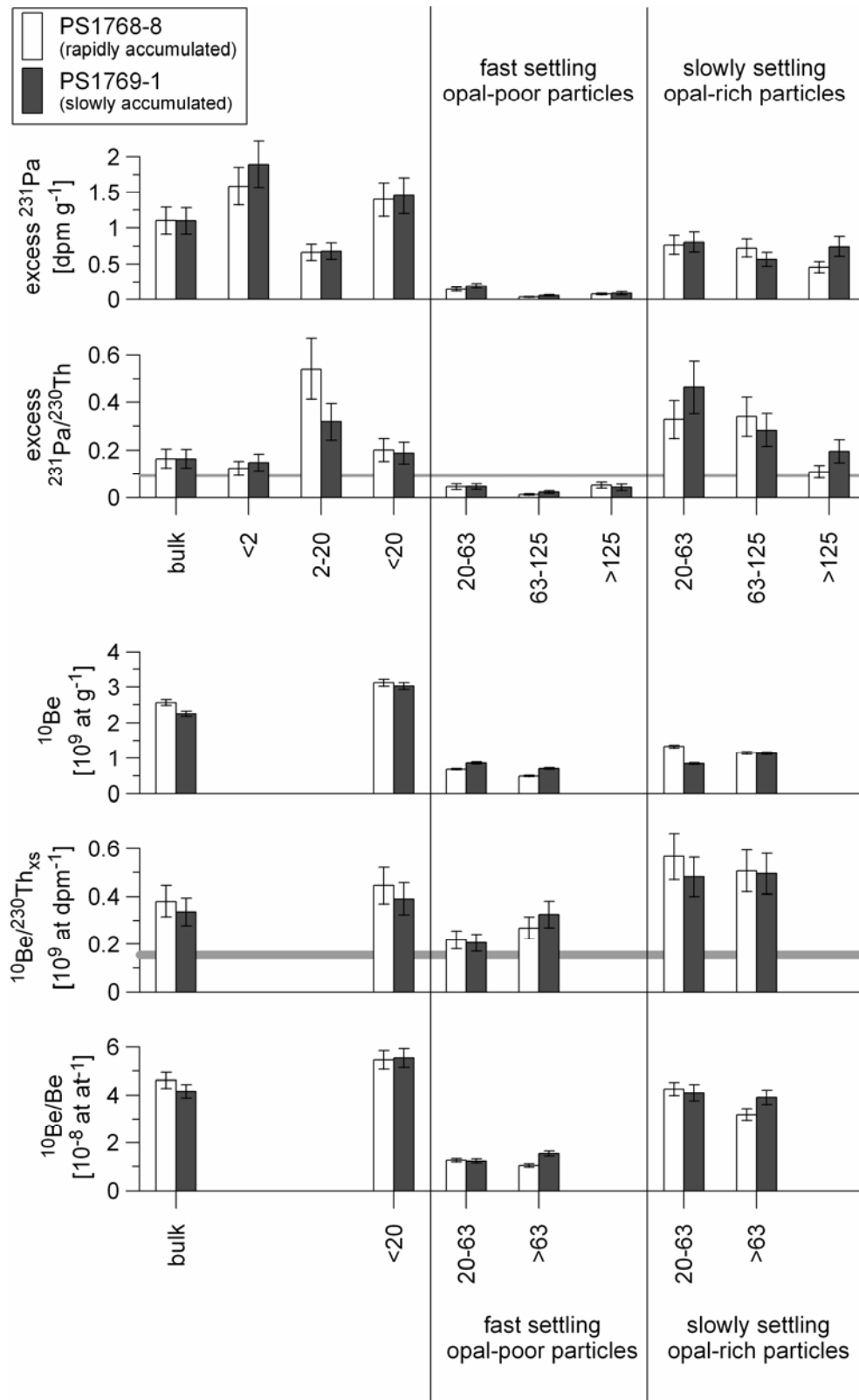


Figure 2

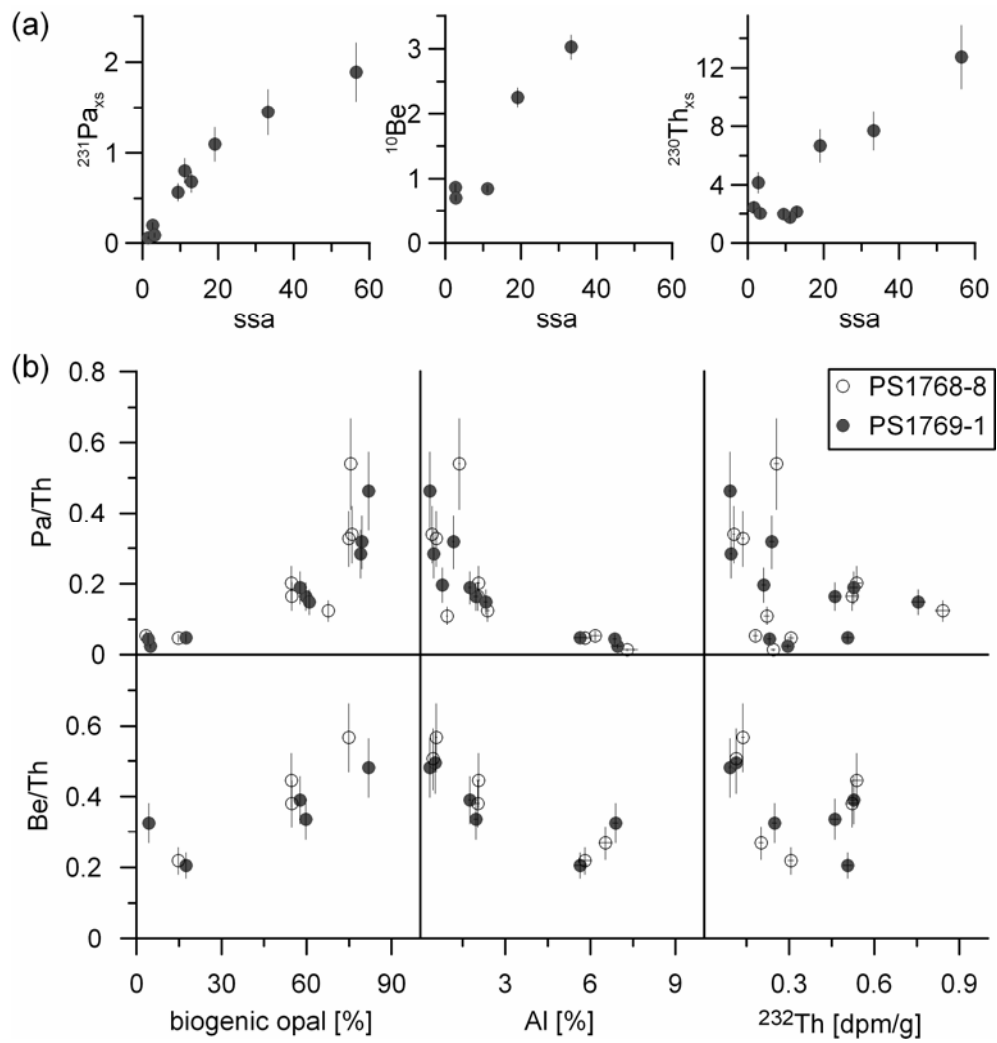


Figure 3

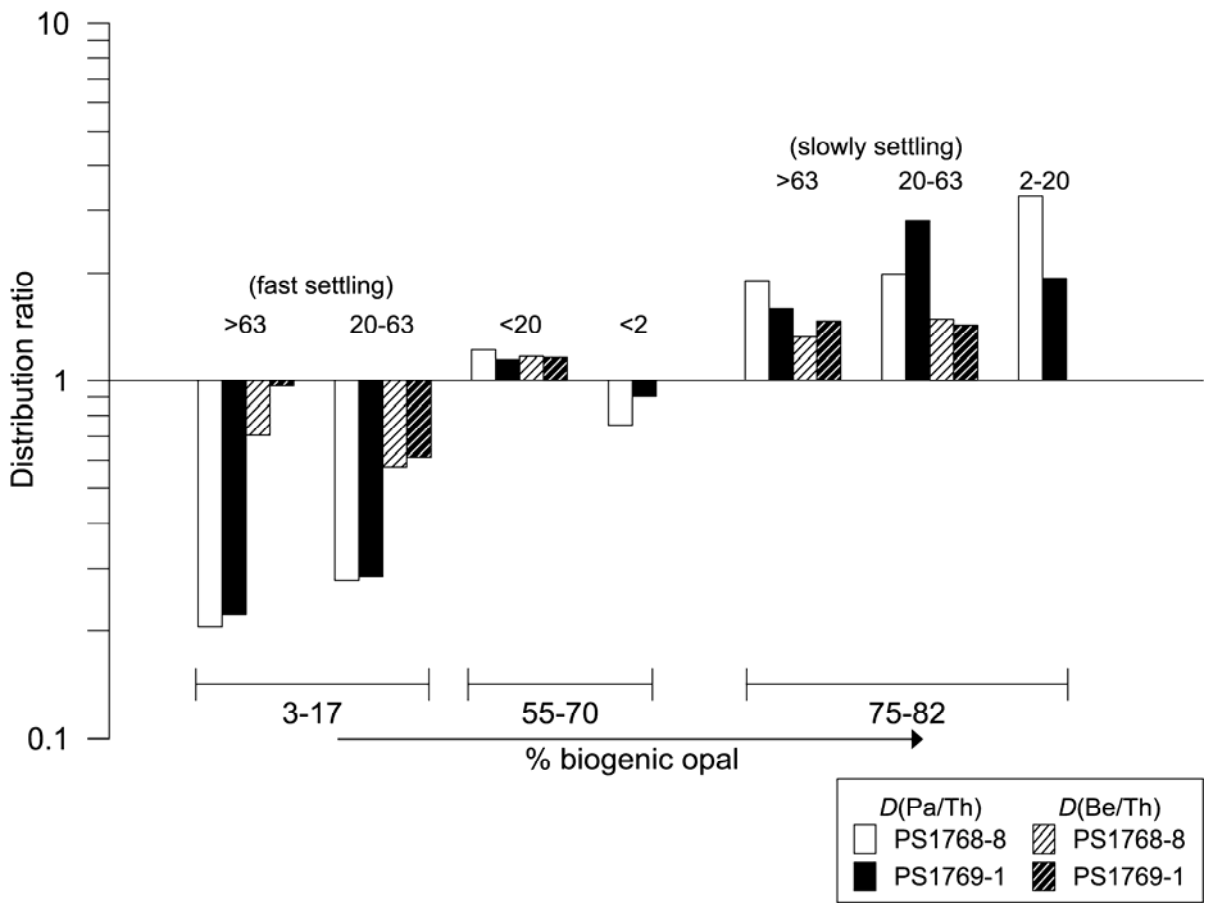


Figure 4

